

Robust and Efficient Fine-tuning of LLMs with Bayesian Reparameterization of Low-Rank Adaptation

Ayan Sengupta^{*, \diamond}

Indian Institute of Technology Delhi, India

AYAN.SENGUPTA@EE.IITD.AC.IN

Vaibhav Seth^{*}

Indian Institute of Technology Delhi, India

VAIBHAV.SETH.MT121@MATHS.IITD.AC.IN

Arinjay Pathak^{*}

Indian Institute of Technology Delhi, India

ARINJAY11020@GMAIL.COM

Natraj Raman

JPMorgan AI Research

NATRAJ.RAMAN@JPMORGAN.COM

Sriram Gopalakrishnan

JPMorgan AI Research

SRIRAM.GOPALAKRISHNAN@JPMCHASE.COM

Tanmoy Chakraborty ^{\diamond}

Indian Institute of Technology Delhi, India

TANCHAK@IITD.AC.IN

Abstract

Large Language Models (LLMs) are highly resource-intensive to fine-tune due to their enormous size. While low-rank adaptation is a prominent parameter-efficient fine-tuning approach, it suffers from sensitivity to hyperparameter choices, leading to instability in model performance on fine-tuning downstream tasks. This paper highlights the importance of effective parameterization in low-rank fine-tuning to reduce estimator variance and enhance the stability of final model outputs. We propose **MonteCLoRA**, an efficient fine-tuning technique, employing Monte Carlo estimation to learn an unbiased posterior estimation of low-rank parameters with low expected variance, which stabilizes fine-tuned LLMs with only $\mathcal{O}(1)$ additional parameters. **MonteCLoRA** shows significant improvements in accuracy and robustness, achieving up to 3.8% higher accuracy and 8.6% greater robustness than existing efficient fine-tuning methods on natural language understanding tasks with pre-trained RoBERTa-base. Furthermore, in generative tasks with pre-trained LLaMA-1-7B, **MonteCLoRA** demonstrates robust zero-shot performance with 50% lower variance than the contemporary efficient fine-tuning methods. The theoretical and empirical results presented in the paper underscore how parameterization and hyperpriors balance exploration-exploitation in the low-rank parametric space, therefore leading to more optimal and robust parameter estimation during efficient fine-tuning.

Keywords: Efficient Fine-tuning, Robust Parameterization, Bayesian Parameterization, Monte Carlo Methods, Large Language Models

1 Introduction

The rise of large language models (LLMs) has initiated a transformative shift in natural language processing, revolutionizing an extensive array of tasks (Zhao et al., 2023). Vaswani

^{*}. Equal contribution

^{\diamond} . Corresponding author

et al. (2017) introduced the self-attention-based Transformer architecture, which is capable of efficient handling of long-range dependencies in texts than prior methods that relied on recurrent neural networks (RNNs) and convolutional neural networks (CNNs). Since then, a monumental shift has begun in developing Transformer-based pre-trained language models (PLMs) for solving a wide range of tasks involving natural languages. Over the past few years, the size of these PLMs has dramatically increased from multi-million parameter BERT (Devlin et al., 2018), RoBERTa (Liu et al., 2019), T5 (Raffel et al., 2020) models to recently developed multi-billion parameter LLaMA (Touvron et al., 2023), Falcon (Almazrouei et al., 2023) and Mistral (Jiang et al., 2023) models. Scaling laws of language models (Kaplan et al., 2020) suggest that the superior performance of these models scales with pre-training data size and the required computation. With deeper and larger models and more extensive pre-training, these models exhibit emerging properties such as zero-shot and few-shot in-context learning (Brown et al., 2020), complex reasoning and generalization capabilities. Despite these emerging properties, LLMs still require fine-tuning on downstream tasks for competitive performance (Liu et al., 2022a) and domain and task adaptation.

Given their enormous size and computational requirements, fine-tuning LLMs on every downstream task is often unrealistic and computationally infeasible. For feasibly fine-tuning LLMs, parameter-efficient fine-tuning (PEFT) techniques such as Adapters (Houlsby et al., 2019), selective fine-tuning (Zaken et al., 2021) and low-rank adaptation (Hu et al., 2022) have become immensely popular. Among these PEFT methods, low-rank adaptation (LoRA) has garnered significant attention due to its flexibility, adaptiveness and ability to mitigate catastrophic forgetting during fine-tuning. LoRA reparameterizes pre-trained model weights to a lower dimension, such that only the low-rank matrices are tuned during fine-tuning, keeping the weights of the original pre-trained model frozen. The low-rank decomposition significantly reduces the number of trainable parameters during fine-tuning, offering great computational benefits. For instance, with a latent rank of 8, the number of trainable parameters of a RoBERTa-base (Liu et al., 2019) model can be reduced by 99% (from 110M to 0.3M) with LoRA. Despite its effectiveness, recent studies (Liu et al., 2022b; Valipour et al., 2022; Biderman et al., 2024) showed that LoRA is very sensitive to hyperparameters like learning rate and training batch size and often requires longer training iterations for convergence. Figure 1 illustrates the performance of full fine-tuning (where we fine-tune the whole pre-trained LLM) and LoRA fine-tuning on different natural language understanding tasks with the pre-trained RoBERTa-base model under different learning rates and training batch sizes. The results highlight that the distribution spread for accuracy (different between maximum and minimum accuracy) on the validation dataset can go up to 17 and 24 points for LoRA and full fine-tuning, respectively. Although the inter-quartile range (IQR) for LoRA remains modest for most of the tasks, the high distribution spreads suggest that LoRA is very sensitive to marginal cases. These preliminary results highlight that careful consideration of hyperparameter selection is necessary to balance adapting new knowledge and preserving the pre-trained knowledge. The most obvious way to figure out the most appropriate hyperparameters is to perform extensive hyperparameter tuning (Tribes et al., 2023; Xie et al., 2024). However, unlike small-scale machine learning models, performing grid or random search within the hyperparameter space of LLMs is very costly and impractical. Bayesian methods (Wilson and Izmailov, 2020; Wang

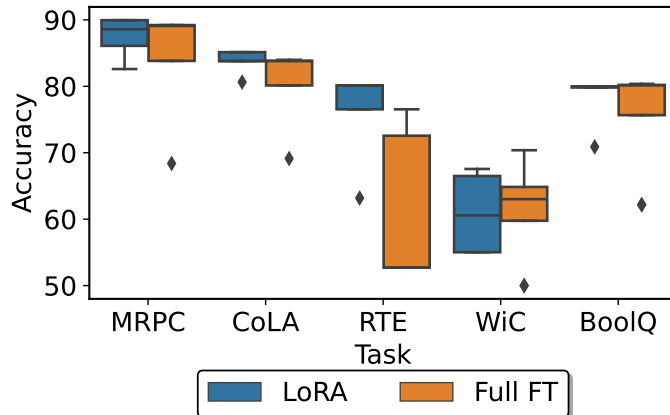


Figure 1: Distribution of validation accuracy of a pre-trained RoBERTa-base model under different learning rates and batch sizes for fine-tuning. We highlight the distributions for full fine-tuning (denoted by Full FT) and low-rank adaptation (denoted by LoRA). LoRA is generally less sensitive to hyperparameters than full fine-tuning as it keeps the original model parameters frozen during fine-tuning. However, the high distribution spread of accuracy (difference between maximum and minimum accuracy) for both the fine-tuning strategies are worth noting and need to be remedied.

and Yeung, 2020), on the other hand, offer an organized solution to hyperparameter sensitivity by marginalizing the predictive distribution. Through appropriate knowledge priors, Bayesian methods diminish the importance of hyperparameter tuning (Papamarkou et al., 2024a) and offer robust alternatives to post-hoc regularization techniques while training on small datasets.

Motivated by the advantages of Bayesian methodologies, we propose a robust low-rank adaptation method for fine-tuning LLMs efficiently. Contrary to the existing sensitivity studies of LoRA, our work provides a structured overview of the challenges faced by LoRA and the full fine-tuning method and proposes a systematic approach to mitigate these challenges. To overcome the sensitivity challenges of LoRA fine-tuning, we propose a Monte Carlo-enhanced low-rank adaptation method, **MonteCLoRA**, which learns posterior distributions of low-rank parameters with appropriate prior distributions. **MonteCLoRA** parameterizes the low-rank parameters as a mixture of multivariate Gaussian distributions, where each distribution’s precision matrix is assumed to follow Wishart knowledge prior. Through Monte Carlo estimation from multiple parameters sampled from the parameter space, **MonteCLoRA** stabilizes the reparametrized parameters and generates robust and unbiased low-rank adaptation for LLMs.

Our theoretical and empirical results justify the importance of parameterization for low-rank adaptation of LLMs. We perform thorough empirical analysis with five natural language understanding (NLU) and six natural language generation (NLG) tasks with two pre-trained LLMs — RoBERTa-base (Liu et al., 2019) and LLaMA-1-7B (Touvron et al., 2023). Empirical results on NLU tasks suggest that **MonteCLoRA** is more stable, where the average spread of accuracy distribution is 10% lower than LoRA and 50% lower than full fine-tuning. In terms of the robustness metrics, **MonteCLoRA** is 5% more robust and achieves

2% better accuracy than LoRA fine-tuning. Remarkably, on NLG tasks, **MonteCLoRA** has 50% lower spread (2.19 points) than LoRA (4.69 points) with zero-shot validation accuracy distribution. Our further in-depth analysis highlights the superiority of **MonteCLoRA** in terms of stable and faster convergence while fine-tuning LLMs.

The key contributions of our work can be summarized as follows¹:

- Our work provides an in-depth theoretical analysis of the impact of hyperparameters on fine-tuning LLMs and highlights the key challenges with low-rank adaptation techniques. To the best of our knowledge, no comprehensive study exists on the sensitivity analysis of LLM fine-tuning.
- We propose a Bayesian alternative to the low-rank adaptation of LLMs for estimating trainable parameters during fine-tuning. The paper theoretically justifies the robustness of the posterior estimation.
- The proposed fine-tuning method adds only $\mathcal{O}(1)$ additional parameters for posterior estimation and is shown to be effective in terms of both performance and stability of the fine-tuned LLMs.
- We provide a thorough empirical study where we demonstrate the effectiveness of the proposed fine-tuning methods with two pre-trained language models – RoBERTa-base and LLaMA-1-7B on five NLU and six NLG (commonsense reasoning) tasks.

The paper is organized as follows. Section 2 describes the related work on efficient fine-tuning strategies for LLMs. Section 3 elaborates on the background concepts used in the paper. In Section 4, we describe our proposed method, **MonteCLoRA**, along with the theoretical results obtained in this work. Section 5 describes the experimental details used in the empirical study done in the paper. In Section 6, we present the results of the empirical study. Section 7 highlights few case studies to analyze robust fine-tuning of LLMs. Additional background materials and supplementary results are furnished in the appendix.

2 Related Work

In this section we briefly describe the related work around robust fine-tuning of LLMs. We divide this section into three broad subjects – (1) fine-tuning methods for LLMs, (2) efficient fine-tuning methods, and (3) Bayesian methods for robust fine-tuning.

Fine-tuning LLMs. Fine-tuning refers to continually training PLMs on a smaller, task-specific dataset. Fine-tuning allows the model to adapt its generalized capabilities to perform better on particular tasks, domains or applications that are not prevalent during the pre-training phase. For the given task-specific training data $Z = \{(x_i, y_i)\}$, in full fine-tuning of LLMs, the model starts with pre-trained weights Φ_0 and updates to $\Phi = \Phi_0 + \Delta\Phi$ by maximizing the conditional language modeling objective

$$\max_{\Phi} \sum_{(x,y) \in Z} \sum_{t=1}^{|y|} \log P_{\Phi}(y_t | x, y_{<t}).$$

1. The source code of **MonteCLoRA** is made available at <https://github.com/LCS2-IIITD/MonteCLoRA>.

In one of the foundation works, Devlin et al. (2018) demonstrated that models pre-trained on large text corpora could be fine-tuned with just one additional output layer to perform a wide range of tasks, effectively transferring learned knowledge to specific tasks. Howard and Ruder (2018) introduced the concept of universal model fine-tuning, emphasizing the importance of discriminative fine-tuning and gradual unfreezing for each model layer to adapt effectively to different downstream tasks. This approach helps in mitigating the catastrophic forgetting problem often observed in LLMs. However, as the models became larger and more capable, fully fine-tuning LLMs turned out to be more computationally infeasible.

Parameter-efficient methods of fine-tuning. PEFT aims to adapt large PLMs to specific tasks by optimizing a small subset of the model’s parameters rather than undertaking the computationally expensive training of the entire pre-trained model. These techniques significantly reduce the computational overhead and memory usage typically associated with fine-tuning large models. There are three broad classes of PEFT techniques – additive, selective and reparameterization-based. Additive PEFT strategies (Houlsby et al., 2019; Pfeiffer et al., 2020) modify the underlying model’s architecture by injecting new additive trainable parameters. Selective PEFT methods (Zaken et al., 2021; Sung et al., 2021) select a subset of parameters for fine-tuning, and the rest remain frozen. On the other hand, reparameterization-based PEFT methods introduce low-dimensional reparameterized parameters for fine-tuning.

One of the most prominent efficient fine-tuning methods, LoRA (Hu et al., 2022), uses low-rank reparameterization to reduce the learnable parameter space to a lower-dimensional space. Subsequently, several alternatives of LoRA have been proposed, mostly keeping efficiency and downstream performance in focus. One such method, AdaLoRA (Zhang et al., 2023), dynamically allocates parameter budgets among weight matrices based on their importance, employing singular value decomposition to optimize incremental updates. Sparse LoRA (SoRA) extends LoRA by incorporating a gate unit optimized with a proximal gradient method (Ding et al., 2023), allowing dynamic adjustments to the intrinsic rank during training and effectively controlling the sparsity of updates. DoRA (Liu et al., 2024) decomposes the pre-trained weight into magnitude and direction components for fine-tuning, utilizing LoRA for efficient directional updates, which enhances both the learning capacity and training stability without increasing inference overhead. Although these PEFT methods demonstrate superior downstream performance in terms of extrinsic metrics like accuracy, these methods are susceptible to task-specific configurations. For instance, SoRA depends on tuning the sparsity controls, introducing instability during training due to abrupt changes in sparsity levels. Moreover, these methods often overfit when fine-tuned on small datasets and generate overconfident predictions during inference (Yang et al., 2024; Agarwal et al., 2024; Sengupta et al., 2024).

Bayesian Methods for Model Robustness. Bayesian frameworks are particularly effective in handling model uncertainty (Daxberger et al., 2021; Zhang et al., 2021; Deng et al., 2022), offer a robust solution to this issue by enabling a probabilistic interpretation of model weights, which helps in assessing the uncertainty of the predictions. Papamarkou et al. (2024b) strongly argued that Bayesian deep learning is more favorable over similar frequentist alternatives. This is because Bayesian methods provide advantages that can help overcome many of the challenges that deep learning faces. Bayesian deep learning

is known to reduce the importance of hyperparameter tuning by incorporating relevant hyper-priors. Bayesian deep learning is also known to enable domain knowledge priors, as opposed to post-hoc regularization on small datasets. Uncertainty quantification is another aspect where Bayesian methods gain an advantage over the alternative frequentist methods by using it to improve the reliability of the decision-making process, which helps the model generalize better on out-of-distribution inputs. Also, by dynamically updating prior beliefs in response to new evidence, Bayesian frameworks allow selective retention of valuable information from previous tasks while adapting to new ones. This mitigates the issue of model decay, which occurs in static models, assuming that underlying data patterns remain constant over time. In a recent development, Laplace-LoRA (Yang et al., 2024), a Bayesian post-hoc treatment of LoRA was introduced that leverages Laplace approximation to estimate the posterior distributions of the parameters involved in the low-rank adaptations, significantly improving the calibration of fine-tuned models. Albeit a robust solution to the overconfidence problem of PEFT methods, Laplace-LoRA is a post-hoc calibration method requiring longer training iterations to bring the low-rank parameters from an unstable basin (a subspace with associated with same local optimum) to a more stable parametric space. Therefore, Laplace-LoRA often leads to sub-optimal downstream performance.

Uniqueness of MonteCLoRA. Our method balances performance and stability through Monte Carlo estimation over the low-dimensional parametric space. With appropriate parametric assumptions, MonteCLoRA can provide an unbiased and robust estimate for the posterior distribution, providing excellent stability and performance gain. Moreover, unlike existing Bayesian methods like Laplace-LoRA, MonteCLoRA can be used on both ad-hoc and post-hoc basis and, therefore, can follow the same optimization path as the other PEFT methods to learn the reparameterized model parameters, ensuring better flexibility and adaptiveness.

3 Background

In this section we elaborate on the concepts of LoRA for fine-tuning LLMs. We also lay down the theoretical motivation behind robust low-rank parameterization. All the mathematical notations used in this section are summarized in Table 1.

3.1 LoRA for Fine-tuning LLMs

LoRA leverages low-rank matrix decomposition to incorporate trainable parameters that adapt the pre-trained model’s weights in a parameter-efficient manner. Consider a pre-trained weight matrix $\mathbf{W}_0 \in \mathbb{R}^{n_{\text{out}} \times n_{\text{in}}}$. LoRA constrains its update by expressing it through a low-rank decomposition as follows:

$$\mathbf{W} = \mathbf{W}_0 + \Delta\mathbf{W} = \mathbf{W}_0 + \mathbf{B}\mathbf{A},$$

where $\mathbf{B} \in \mathbb{R}^{n_{\text{out}} \times r}$, $\mathbf{A} \in \mathbb{R}^{r \times n_{\text{in}}}$, and the rank $r \ll \min(n_{\text{in}}, n_{\text{out}})$. During training, \mathbf{W}_0 remains frozen and is not subject to gradient updates, while the matrices, \mathbf{A} and \mathbf{B} , contain the trainable parameters. Both \mathbf{W}_0 and $\Delta\mathbf{W} = \mathbf{B}\mathbf{A}$ are applied to the same input, and their resulting output vectors are summed element-wise. This approach allows LoRA to efficiently adapt large pre-trained models to new tasks with a relatively small number of additional parameters. Figure 2 provides a pictorial illustration of LoRA.

Notation Type	Notation	Description
Low-rank adaptation	\mathbf{W}_0	Pre-trained weight matrix
	n_{in}	Input dimensions of \mathbf{W}_0
	n_{out}	Output dimensions of \mathbf{W}_0
	r	LoRA rank
	\mathbf{A}	LoRA A matrix
	\mathbf{B}	LoRA B matrix
Optimization	J	Objective or loss function
	θ	Model parameters
	∇J	Gradient of the loss function
	L	Lipschitz constant of the loss function
	σ	Standard deviation bound of the stochastic gradients
	ρ	Stochastic noise in the gradient
	\mathbf{H}	Hessian matrix of the loss function
	λ	Eigenvalue of a matrix
	ξ	Point for mean value theorem
	γ	Gaussian random variable added to the model parameter
	Λ_{max}	Maximum eigenvalue of Hessian

Table 1: Glossary of all the mathematical notations used in Section 3.

3.2 Sensitivity of Gradient Descent to Hyperparameters

Stochastic gradient descent (SGD) is a widely popular optimization technique for training neural networks. In SGD, we calculate the gradient of the training objective function with respect to the learnable neural parameters on a sample training batch and iteratively update the parameters towards the edge of a basin of optima, as shown by Izmailov et al. (2019), where the training objective is minimized. In this section, we describe some of the properties of SGD to understand how different hyperparameters such as optimizer learning rate impacts the optimization process.

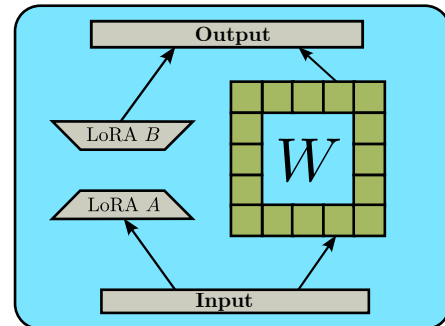


Figure 2: Illustration of the LoRA fine-tuning framework.

3.2.1 CONVERGENCE OF SGD AND THE LIPSCHITZ CONSTANT

The convergence of SGD is known to depend on the Lipschitz constant through its influence on the choice of step sizes. Several studies have established an inverse relationship between the maximum step sizes that ensure convergence and the learning rate.

Ghadimi and Lan (2013), in their seminal work, demonstrated that selecting the learning rate within a specific range guarantees the convergence of the SGD algorithm, based on foundational assumptions in stochastic optimization. These key assumptions include,

1. **Lipschitz-Continuous Gradient.** The gradient ∇J of the objective function $J : \mathbb{R}^n \rightarrow \mathbb{R}$ is Lipschitz continuous with a constant $L > 0$,

$$\|\nabla J(\mathbf{X}) - \nabla J(\mathbf{Y})\| \leq L\|\mathbf{X} - \mathbf{Y}\|, \quad \forall \mathbf{X}, \mathbf{Y} \in \mathbb{R}^n.$$

2. **Bounded Variance of Stochastic Gradients.** The variance of the stochastic gradients $g(x, \rho)$ is bounded, i.e.,

$$\mathbb{E}_\rho [\|g(\mathbf{X}, \rho) - \nabla J(\mathbf{X})\|^2] \leq \sigma^2, \quad \forall x \in \mathbb{R}^n,$$

where ρ represents the stochastic noise in the gradient.

Under these assumptions, it is shown that choosing the step sizes $\in \left(0, \frac{2}{L}\right)$ ensures convergence. Specifically, the expected squared norm of the gradient at a randomly selected iterate diminishes at the rate,

$$\mathbb{E} [\|\nabla J(\mathbf{X}_R)\|^2] = O\left(\frac{1}{\sqrt{T}}\right),$$

where T is the number of iterations and R is chosen uniformly at random from $\{1, 2, \dots, T\}$. This result implies that by setting the learning rate within the specified range determined by the Lipschitz constant L , the SGD algorithm converges to a stationary point at a sub-linear rate, even in non-convex settings. Analysis by Garrigos and Gower (2024) provides a detailed exploration of the convergence of stochastic gradient methods, along with bounds on the learning rate. They similarly highlight an inverse relationship between the range of learning rates that guarantee convergence and the Lipschitz constant.

3.2.2 LEMMAS ON LIPSCHITZ CONSTANT OF GRADIENT VECTORS

Lemma 1 *Let $J : \mathbb{R}^n \rightarrow \mathbb{R}$ be a twice continuously differentiable function. Then the gradient ∇J is Lipschitz continuous with Lipschitz constant L equal to the supremum of the maximum eigenvalue of its Hessian matrix $H(\mathbf{X}) = \nabla^2 J(\mathbf{X})$*

$$L = \sup_{x \in \mathbb{R}^n} \lambda_{\max}(H(\mathbf{X})). \tag{1}$$

Proof Let $\mathbf{X}, \mathbf{Y} \in \mathbb{R}^n$ be arbitrary points. By the Mean Value Theorem for vector-valued functions, there exists a point $\boldsymbol{\xi}$ lying on the line segment connecting \mathbf{X} and \mathbf{Y} such that

$$\nabla J(\mathbf{X}) - \nabla J(\mathbf{Y}) = H(\boldsymbol{\xi})(\mathbf{X} - \mathbf{Y}). \tag{2}$$

Taking the norm on both sides, we have,

$$\|\nabla J(\mathbf{X}) - \nabla J(\mathbf{Y})\| = \|H(\boldsymbol{\xi})(\mathbf{X} - \mathbf{Y})\|. \tag{3}$$

Using the submultiplicative property of norms, specifically the operator norm for matrices and the Euclidean norm for vectors, we obtain

$$\|H(\boldsymbol{\xi})(\mathbf{X} - \mathbf{Y})\| \leq \|H(\boldsymbol{\xi})\| \cdot \|\mathbf{X} - \mathbf{Y}\|, \tag{4}$$

where $\|H(\boldsymbol{\xi})\|$ denotes the operator norm (spectral norm) of the Hessian matrix $H(\boldsymbol{\xi})$. Since $H(\boldsymbol{\xi})$ is symmetric (because J is twice continuously differentiable), its operator norm equals its largest eigenvalue in absolute value

$$\|H(\boldsymbol{\xi})\| = \lambda_{\max}(H(\boldsymbol{\xi})). \tag{5}$$

Therefore, we have,

$$\|\nabla J(\mathbf{X}) - \nabla J(\mathbf{Y})\| \leq \lambda_{\max}(H(\boldsymbol{\xi})) \cdot \|\mathbf{X} - \mathbf{Y}\|. \quad (6)$$

Since $\boldsymbol{\xi}$ lies on the line segment between \mathbf{X} and \mathbf{Y} , and \mathbf{X} and \mathbf{Y} are arbitrary in \mathbb{R}^n , we can take the supremum over all such $\boldsymbol{\xi}$

$$\|\nabla J(\mathbf{X}) - \nabla J(\mathbf{Y})\| \leq \left(\sup_{\boldsymbol{\xi} \in \mathbb{R}^n} \lambda_{\max}(H(\boldsymbol{\xi})) \right) \|\mathbf{X} - \mathbf{Y}\|. \quad (7)$$

Thus, the Lipschitz constant L of the gradient ∇J is given by

$$L = \sup_{\mathbf{X} \in \mathbb{R}^n} \lambda_{\max}(H(\mathbf{X})). \quad (8)$$

■

Lemma 2 *Let $J(\boldsymbol{\theta})$ be the loss function over trainable model parameters $\boldsymbol{\theta} \in \mathbb{R}^n$, and $\boldsymbol{\gamma}$ represents Gaussian noise with zero mean. We define the expected loss function as $\tilde{J}(\boldsymbol{\theta}) = \mathbb{E}_{\boldsymbol{\gamma}}[J(\boldsymbol{\theta} + \boldsymbol{\gamma})]$. We also define $\mathbf{H}(\boldsymbol{\theta})$ as the Hessian matrix for $J(\boldsymbol{\theta})$ and $\tilde{\mathbf{H}}(\boldsymbol{\theta})$ as the Hessian matrix for $\tilde{J}(\boldsymbol{\theta})$. Then the maximum eigenvalue of $\tilde{\mathbf{H}}(\boldsymbol{\theta})$ at any given $\boldsymbol{\theta}$ is less than the maximum eigenvalue of $\mathbf{H}(\boldsymbol{\theta})$ over all $\boldsymbol{\theta} \in \mathbb{R}^n$.*

Proof The smoothed loss function $\tilde{J}(\boldsymbol{\theta})$ can be expanded as,

$$\tilde{J}(\boldsymbol{\theta}) = \int J(\boldsymbol{\theta} + \boldsymbol{\gamma}) \mathcal{N}(\boldsymbol{\gamma}; 0, \boldsymbol{\Sigma}) d\boldsymbol{\gamma}.$$

The gradient of $\tilde{J}(\boldsymbol{\theta})$ is,

$$\nabla_{\boldsymbol{\theta}} \tilde{J}(\boldsymbol{\theta}) = \int \nabla_{\boldsymbol{\theta}} J(\boldsymbol{\theta} + \boldsymbol{\gamma}) \mathcal{N}(\boldsymbol{\gamma}; 0, \boldsymbol{\Sigma}) d\boldsymbol{\gamma}.$$

The Hessian of $\tilde{J}(\boldsymbol{\theta})$ is,

$$\tilde{H}(\boldsymbol{\theta}) = \nabla_{\boldsymbol{\theta}}^2 \tilde{J}(\boldsymbol{\theta}) = \int \nabla_{\boldsymbol{\theta}}^2 L(\boldsymbol{\theta} + \boldsymbol{\gamma}) \mathcal{N}(\boldsymbol{\gamma}; 0, \boldsymbol{\Sigma}) d\boldsymbol{\gamma}.$$

So, the Hessian is the expectation of the Hessian at $\boldsymbol{\theta}$, i.e.,

$$\tilde{H}(\boldsymbol{\theta}) = \mathbb{E}_{\boldsymbol{\gamma}}[H(\boldsymbol{\theta} + \boldsymbol{\gamma})].$$

Since $H(\boldsymbol{\theta})$ is symmetric and positive semi-definite (for convex L), so is $H(\boldsymbol{\theta} + \boldsymbol{\gamma})$ for all $\boldsymbol{\gamma}$. The expected Hessian $\tilde{H}(\boldsymbol{\theta})$ is a convex combination (integral) of Hessians at points $\boldsymbol{\theta} + \boldsymbol{\gamma}$. Therefore, $\tilde{H}(\boldsymbol{\theta})$ is also symmetric and positive semi-definite. Let \mathbf{v} be an eigenvector of $\tilde{H}(\boldsymbol{\theta})$ with eigenvalue λ , then,

$$\tilde{H}(\boldsymbol{\theta})\mathbf{v} = \lambda\mathbf{v}.$$

Using the fact that $\mathbf{v}^T \mathbf{v}$ is a scalar, we have,

$$\lambda = \frac{\mathbf{v}^T \tilde{H}(\boldsymbol{\theta}) \mathbf{v}}{\mathbf{v}^T \mathbf{v}} = \frac{\mathbf{v}^T \mathbb{E}_\gamma [H(\boldsymbol{\theta} + \gamma)] \mathbf{v}}{\mathbf{v}^T \mathbf{v}}.$$

Since \mathbb{E} is linear, we have,

$$\lambda = \mathbb{E}_\gamma \left[\frac{\mathbf{v}^T H(\boldsymbol{\theta} + \gamma) \mathbf{v}}{\mathbf{v}^T \mathbf{v}} \right].$$

Let us define

$$S(\boldsymbol{\theta} + \gamma) = \frac{\mathbf{v}^T H(\boldsymbol{\theta} + \gamma) \mathbf{v}}{\mathbf{v}^T \mathbf{v}}.$$

Therefore,

$$\lambda = \mathbb{E}_\gamma [S(\boldsymbol{\theta} + \gamma)].$$

Since $H(\boldsymbol{\theta} + \gamma)$ is positive semi-definite, its eigenvalues $S(\boldsymbol{\theta} + \gamma) \geq 0$. Let Λ_{\max} be the maximum eigenvalue of $H(\boldsymbol{\theta})$ over all $\boldsymbol{\theta}$. Then, for all γ

$$S(\boldsymbol{\theta} + \gamma) \leq \Lambda_{\max}.$$

Taking expectation we get,

$$\lambda = \mathbb{E}_\gamma [S(\boldsymbol{\theta} + \gamma)] \leq \Lambda_{\max}.$$

Hence,

$$\lambda_{\max}(\tilde{H}(\boldsymbol{\theta})) = \sup_{\mathbf{v} \neq 0} \frac{\mathbf{v}^T \tilde{H}(\boldsymbol{\theta}) \mathbf{v}}{\mathbf{v}^T \mathbf{v}} \leq \Lambda_{\max}. \quad \blacksquare$$

3.3 Measuring Robustness of a Fine-Tuning Strategy

The previous section discusses the theoretical underpinning of sensitivity of a fine-tuning strategy. Therefore, it is of immense importance to quantify the sensitivity (or robustness) of a fine-tuning method. Robustness in statistical modeling refers to the ability of a model to perform well and provide reliable results across a wide range of conditions and assumptions. In model fine-tuning, a robust strategy can perform reliably under different hyperparameters affecting the fine-tuning process, such as the learning rate of the optimizer, training batch size, etc. Although robustness measures can be defined differently, we resort to statistical measures to quantify the robustness of different fine-tuning strategies. Suppose a model \mathcal{M} is fine-tuned on a given task \mathcal{T} with two different fine-tuning strategies, $\mathcal{S}^{(1)}$ and $\mathcal{S}^{(2)}$, with hyperparameter settings, $\Lambda_1, \Lambda_2, \dots, \Lambda_k$ and obtains scores $s_1^{(1)}, s_2^{(1)}, \dots, s_k^{(1)}$ and $s_1^{(2)}, s_2^{(2)}, \dots, s_k^{(2)}$, respectively on the validation dataset. Depending on the nature of these scores, we can calculate the metrics to compare the robustness of these fine-tuning strategies. For intrinsic metrics like negative loglikelihood, we calculate *intrinsic robustness* as,

$$\mathcal{R}_{\mathcal{S}^{(1)}} = \frac{1}{\text{med}(\{s_1^{(1)}, s_2^{(1)}, \dots, s_k^{(1)}\})}. \quad (9)$$

Here, med is the median of the score distribution. Similarly, for extrinsic metrics like accuracy, we calculate *extrinsic robustness* as,

$$\mathcal{R}_{\mathcal{S}^{(1)}} = med(\{s_1^{(1)}, s_2^{(1)}, \dots, s_k^{(1)}\}). \quad (10)$$

During model validation, we typically aim for minimizing the intrinsic metrics (for instance, lower validation loss is expected) and maximizing the extrinsic metrics. Therefore, having $\mathcal{R}_{\mathcal{S}^{(1)}} > \mathcal{R}_{\mathcal{S}^{(2)}}$ ensures that the probability of achieving lower intrinsic metric is higher for $\mathcal{S}^{(1)}$ than $\mathcal{S}^{(2)}$, indicating more robustness for $\mathcal{S}^{(1)}$. A similar argument also holds for the extrinsic robustness metric, where a higher score indicates a more robust fine-tuning strategy. As we use the same hyperparameter configurations for comparing different strategies, these robustness metrics allow us to compare different methods without incorporating the variances within the hyperparameters.

3.4 Bayesian Inference and Monte Carlo Estimation Methods

In the Bayesian treatment of machine learning and deep learning models, we are often concerned with the predictive distribution and aim to incorporate prior information into our estimates. Bayesian methods typically regularize the weight space of the model, resulting in a robust reparameterization of the models. With Bayesian formulation, we can parameterize the probability distribution of a model parameter θ as,

$$P(\theta) = \int P(\theta | \beta)P(\beta)d\beta \quad (11)$$

where β denotes the parameters that we learn to represent the distribution of the weight space of the model. The integral is often highly intractable due to the complex and high-dimensional nature of the distributions involved. Monte Carlo estimation provides a simple computational algorithm for calculating computationally intractable statistics to calculate analytically. Suppose, given a random variable θ , we want to calculate $\mathbb{E}[\theta]$, where the probability distribution is complex or does not have a closed form solution. Monte Carlo estimate provides a simple computational solution,

$$\hat{\theta} = \frac{1}{N} \sum_{i=1}^N \theta_i, \text{ where } \theta_i \sim P(\theta). \quad (12)$$

Similarly, the integral in Equation 11 can be calculated as,

$$\hat{P}(\theta) = \frac{1}{N} \sum_{i=1}^N P(\theta | \beta_i), \text{ where } \beta_i \sim P(\beta). \quad (13)$$

Lemma 3 *Monte Carlo estimate is an unbiased estimator of θ , i.e., $\mathbb{E}[\hat{\theta}] = \mathbb{E}[\theta]$.*

Proof

$$\mathbb{E}[\hat{\theta}] = \mathbb{E}\left[\frac{1}{N} \sum_{i=1}^N \theta_i\right] \implies \mathbb{E}[\hat{\theta}] = \frac{1}{N} \sum_{i=1}^N \mathbb{E}[\theta_i]$$

Notation	Description
θ_i	i -th column vector in the low-rank matrix
μ_i	i -th column mean vector
\mathcal{W}	Wishart Distribution
V	Scale matrix of Wishart distribution
Σ	Sampled covariance matrix
Dir	Dirichlet Distribution
α	Dirichlet distribution concentration parameter
Π	Mixture weights vector
π_k	k -th mixture weight
N	Number of inner Monte Carlo samples
M	Number of outer Monte Carlo samples
$\mathbf{W}_{stochastic}$	Stochastic component sampled from the Monte Carlo process
ϵ	Sample scaler

Table 2: Glossary of all the mathematical notations used with MonteCLoRA.

Since θ_i is i.i.d, and $\mathbb{E}[\theta_i] = \mathbb{E}[\theta]$,

$$\mathbb{E}[\hat{\theta}] = \mathbb{E}[\theta].$$

Hence, the Monte Carlo estimate is an unbiased estimate of θ . ■

4 Proposed Methodology

In this section, we introduce our proposed method, **MonteCLoRA**, a **Monte Carlo enhanced Low-Rank Adaptation** for fine-tuning LLMs. It learns a posterior distribution for each low-rank \mathbf{A} parameter and estimates a robust and unbiased posterior estimator. With Monte Carlo estimation, **MonteCLoRA** prevents mode collapse of the low-rank parameters, instead learns to sample from a basin of optima for improved generalization and robustness. Figure 3 illustrates our overall methodology. Table 2 describes all the mathematical notations to describe **MonteCLoRA**.

4.1 Gaussian Factorization of Weight Space

Learning a posterior distribution over the entire weight space of a model is a complex and computationally demanding task. To address this, we adopt a factorization assumption, where we presume that the model’s weight space distribution can be decomposed into the product of the distributions across all layers. This approach decouples the posterior distribution learning of one weight matrix from others, enabling efficient posterior estimation.

Our primary focus is on low-rank matrices, though this methodology extends to full-rank matrices. Suppose we have a low-rank weight matrix $\theta \in \mathbb{R}^{r \times n_{in}}$. We denote the probability distribution of its weight space as $P(\theta)$. A key assumption is that each of the n_{in} column vectors ($\theta_i \in \mathbb{R}^r$) independently follows a Gaussian distribution with a shared covariance matrix but with distinct means,

$$P(\theta) = P(\theta_1, \theta_2, \dots, \theta_{n_{in}}) = \prod_{i=1}^{n_{in}} P(\theta_i). \quad (14)$$

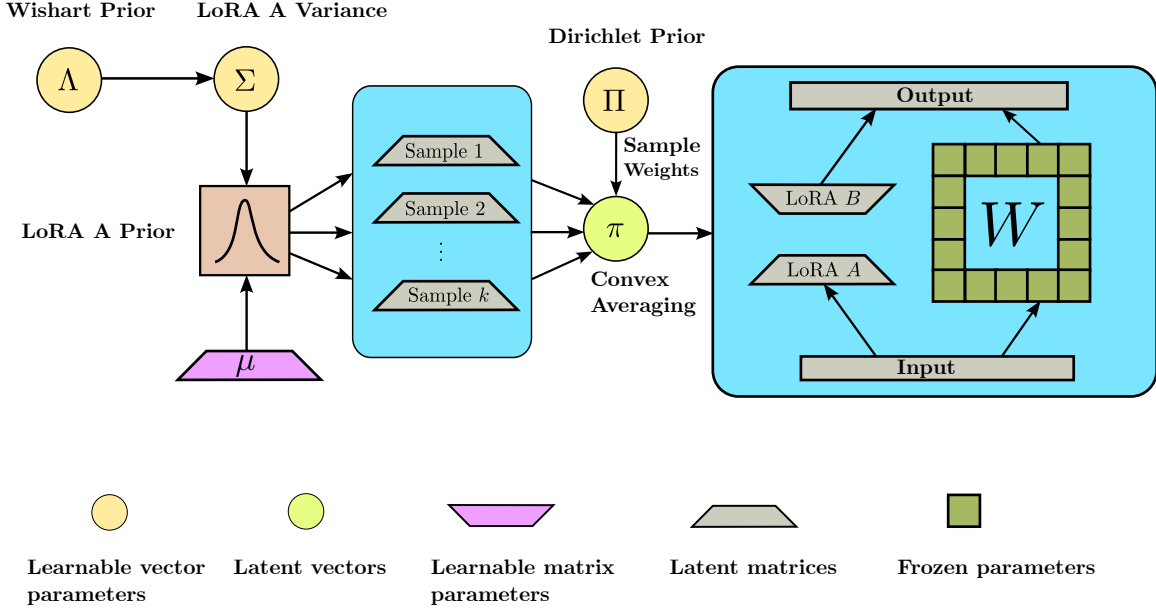


Figure 3: A schematic illustration of our proposed method, MonteCLoRA. The method uses mixture of multivariate Gaussian distributions for robust estimation of LoRA A parameters. Each Gaussian distribution has the LoRA initialized parameter μ as the distribution mean and variance Σ sampled from Wishart prior distribution with learnable scale matrix. The mixture weight parameter π is sampled from a Dirichlet prior distribution.

We parameterize the distribution of each θ_i by assuming that, given a covariance matrix $\Sigma \in \mathbb{R}^{r \times r}$, each θ_i is generated from $\mathcal{N}(\mu_i, \Sigma)$, with μ_i being the corresponding column mean vector. Using a common covariance matrix allows for efficient posterior learning without adding a significant number of additional parameters. The covariance matrix is not a fixed parameter; instead, it is sampled from a Wishart distribution (for details on the distribution, check Appendix A.2) with learnable priors. The learnable prior parameters enable us to explore the low-rank parametric weight space, yielding more robust parameter estimates for the model. We formalize $P(\theta_i)$ as a mixture of multivariate Gaussian distributions,

$$P(\theta_i) = \sum_{k=1}^N \pi_k \cdot \mathcal{N}(\mu_i, \Sigma), \quad \text{s.t.} \quad \sum_{k=1}^N \pi_k = 1. \quad (15)$$

The mixture weights $\Pi = (\pi_1, \pi_2, \dots, \pi_N)$ are drawn from a Dirichlet distribution $\text{Dir}(\alpha)$, with concentration parameter $\alpha = (\alpha_1, \alpha_2, \dots, \alpha_N)$. Each multivariate Gaussian distribution in the mixture shares the same covariance matrix. The mean vector μ_i of each Gaussian distribution is initialized randomly at the start of training (similar to LoRA A matrices) and is subsequently learned. The covariance matrix Σ is sampled from a Wishart prior distribution $\mathcal{W}_r(\mathbf{V}, n_{\text{in}})$, where \mathbf{V} is the learnable scale matrix, n_{in} is the degrees of freedom, and r is the LoRA rank. Given independence across dimensions, we assume \mathbf{V} to

be diagonal. Therefore, using Equations 14 and 15, we can write the joint density as,

$$P(\boldsymbol{\theta}, \boldsymbol{\Pi}, \boldsymbol{\Sigma}) = \prod_{i=1}^{n_{\text{in}}} \left(\sum_{k=1}^N \pi_k \cdot \mathcal{N}(\boldsymbol{\theta}_k; \boldsymbol{\mu}_i, \boldsymbol{\Sigma}) \right) \cdot \text{Dir}(\boldsymbol{\Pi}; \boldsymbol{\alpha}) \cdot \mathcal{W}_r(\boldsymbol{\Sigma}; \mathbf{V}, n_{\text{in}}). \quad (16)$$

Note that different LoRA parameters may use distinct covariance matrices learned with different Wishart scale matrices.

4.2 Monte Carlo Estimation of LoRA Parameters

Given that $\boldsymbol{\Pi}$ and $\boldsymbol{\Sigma}$ are independent, we can simplify the Monte Carlo estimation for the expectation of $\boldsymbol{\theta}_i$. The expectation of $\boldsymbol{\theta}_i$ is,

$$\mathbb{E}[\boldsymbol{\theta}_i] = \int \boldsymbol{\theta}_i P(\boldsymbol{\theta}_i | \boldsymbol{\Pi}, \boldsymbol{\Sigma}) P(\boldsymbol{\Pi}) P(\boldsymbol{\Sigma}) d\boldsymbol{\theta}_i d\boldsymbol{\Pi} d\boldsymbol{\Sigma}. \quad (17)$$

In the Monte Carlo formulation, we approximate this integral by sampling from the distributions of $\boldsymbol{\Pi}$ and $\boldsymbol{\Sigma}$ and then computing the expectation over $\boldsymbol{\theta}_i$, given each sampled pair $(\boldsymbol{\Pi}, \boldsymbol{\Sigma})$.

1. Sample $\boldsymbol{\Pi}$ and $\boldsymbol{\Sigma}$

- (a) Draw M samples $\boldsymbol{\Pi}^{(j)} \sim \text{Dir}(\boldsymbol{\alpha})$, where $j = 1, \dots, M$.
- (b) Draw M samples $\boldsymbol{\Sigma}^{(j)} \sim \mathcal{W}_r(\mathbf{V}, n_{\text{in}})$, where $j = 1, \dots, M$.

2. Sample $\boldsymbol{\theta}_i$ given $\boldsymbol{\Pi}$ and $\boldsymbol{\Sigma}$

For each pair $(\boldsymbol{\Pi}^{(j)}, \boldsymbol{\Sigma}^{(j)})$, sample N values of $\boldsymbol{\theta}_i^{(k,j)} \sim P(\boldsymbol{\theta}_i | \boldsymbol{\Pi}^{(j)}, \boldsymbol{\Sigma}^{(j)})$, where $k = 1, \dots, N$.

3. Compute the Monte Carlo Estimate

Using the samples, the expectation $\mathbb{E}[\boldsymbol{\theta}_i]$ is estimated as:

$$\mathbf{E}[\boldsymbol{\theta}_i] \approx \frac{1}{M} \sum_{j=1}^M \frac{1}{N} \sum_{k=1}^N \boldsymbol{\theta}_i^{(k,j)}. \quad (18)$$

The inner sum $\frac{1}{N} \sum_{k=1}^N \boldsymbol{\theta}_i^{(k,j)}$ approximates the conditional expectation, $\mathbb{E}[\boldsymbol{\theta}_i | \boldsymbol{\Pi}^{(j)}, \boldsymbol{\Sigma}^{(j)}]$. The outer sum averages over the prior samples of $\boldsymbol{\Pi}$ and $\boldsymbol{\Sigma}$, estimating the marginal expectation $\mathbb{E}[\boldsymbol{\theta}_i]$. This two-layer Monte Carlo approach approximates the integral by leveraging the independence of $\boldsymbol{\Pi}$ and $\boldsymbol{\Sigma}$ and sampling $\boldsymbol{\theta}_i$ conditioned on each sampled pair $(\boldsymbol{\Pi}, \boldsymbol{\Sigma})$. The independence assumption permits separate sampling for each $\boldsymbol{\theta}_i$, combined into a final sampled weight matrix.

Algorithm 1 formalizes the forward method of MonteCLoRA for each LoRA parameter initialized with $\boldsymbol{\mu}$. The learnable parameters in the above approach are the LoRA parameters, Wishart distribution scale matrix \mathbf{V} and the Dirichlet concentration parameter $\boldsymbol{\alpha}$. The Wishart distribution scale is a diagonal matrix of order n_{out} , and the Dirichlet concentration is another vector of size N . Hence, for each MonteCLoRA layer, we add $n_{\text{out}} + N$

Algorithm 1 MonteCLoRA forward method

Require: n_{in} : Input feature size
Require: n_{out} : Output feature size
Require: N : Number of mixture components
Require: $\mathbf{V} \in \mathbb{R}^{n_{\text{out}} \times n_{\text{out}}}$: Wishart Distribution Prior (Trainable Diagonal Matrix)
Require: $\boldsymbol{\alpha} \in \mathbb{R}^N$: Dirichlet Distribution Prior (Trainable Vector)
Require: $\boldsymbol{\mu} \in \mathbb{R}^{n_{\text{in}} \times n_{\text{out}}}$: Weight matrix of the linear layer (Trainable Dense Matrix)
Require: ϵ : Sample Scaler
Ensure: Updated weight matrix $\tilde{\boldsymbol{\mu}}$

$\hat{\boldsymbol{\Sigma}} \sim \mathcal{W}_{n_{\text{out}}}(\mathbf{V}, n_{\text{in}})$	▷ Sample from Wishart Distribution
$\pi_1, \pi_2, \dots, \pi_N \sim \text{Dir}(\boldsymbol{\alpha})$	▷ Sample from Dirichlet Distribution
$\hat{\mathbf{S}}_1, \hat{\mathbf{S}}_2, \dots, \hat{\mathbf{S}}_N \sim \mathcal{N}(\mathbf{0}, \hat{\boldsymbol{\Sigma}})$	▷ Sample from multivariate Gaussian distribution
$\mathbf{W}_{\text{stochastic}} \leftarrow \sum_{i=1}^N \pi_i \cdot \hat{\mathbf{S}}_i$	▷ Compute the Stochastic Component
$\tilde{\boldsymbol{\mu}} \leftarrow \boldsymbol{\mu} + \epsilon \mathbf{W}_{\text{stochastic}}$	▷ Update Weight Matrix

parameters only. When applied this to LoRA down projection matrix, the number of extra parameters is just $r + N$, and we introduce only a fraction of parameters $\mathcal{O}(\frac{r+N}{n_{\text{in}} \times r})$ obtained from LoRA, which is approximately $\mathcal{O}(1)$ as $r \ll \min(n_{\text{in}}, n_{\text{out}})$, and N are usually of same order which in turn is a only small fraction of total parameters for a layer. Hence, the total number of parameters over the LoRA parameters is very small and $\mathcal{O}(1)$ compared to LoRA parameters.

4.3 Theoretical Results

This section presents the theoretical results involving MonteCLoRA, for demonstrating the effectiveness of Bayesian parameterization for robust fine-tuning of LLMs. We show that MonteCLoRA derives an unbiased and robust estimate of the true model parameters and how it influences and stabilizes the final output obtained by the fine-tuned model.

Lemma 4 *Sample scale factor ϵ shifts the final output proportionally.*

Proof Consider a simplified version of the model where we ignore activations. The neural network can be represented as a product of multiple weight matrices, $\boldsymbol{\theta}_1, \boldsymbol{\theta}_2, \dots, \boldsymbol{\theta}_n$. The output for an input \mathbf{X} is given by,

$$\mathbf{Y} = \boldsymbol{\theta}_1 \boldsymbol{\theta}_2 \cdots \boldsymbol{\theta}_n \mathbf{X}.$$

Now, we consider the parameterization used by MonteCLoRA. Each weight matrix $\boldsymbol{\theta}_i$ includes a scaled random variable added to it. We represent random variables as $\hat{\phi}_i$, and the scaling factor is ϵ . The output for an input \mathbf{X} in this case becomes,

$$\bar{\mathbf{Y}} = (\boldsymbol{\theta}_1 + \epsilon \hat{\phi}_1)(\boldsymbol{\theta}_2 + \epsilon \hat{\phi}_2) \cdots (\boldsymbol{\theta}_n + \epsilon \hat{\phi}_n) \mathbf{X}.$$

Expanding the terms and neglecting $\mathcal{O}(\epsilon^2)$ terms (this assumption is valid as we typically use $\epsilon \in \mathcal{O}(10^{-3})$), we obtain

$$\begin{aligned}\bar{\mathbf{Y}} &= \boldsymbol{\theta}_1 \boldsymbol{\theta}_2 \cdots \boldsymbol{\theta}_n \mathbf{X} + \epsilon \left(\hat{\boldsymbol{\phi}}_1 \boldsymbol{\theta}_2 \cdots \boldsymbol{\theta}_n + \boldsymbol{\theta}_1 \hat{\boldsymbol{\phi}}_2 \boldsymbol{\theta}_3 \cdots \boldsymbol{\theta}_n + \cdots + \boldsymbol{\theta}_1 \boldsymbol{\theta}_2 \cdots \boldsymbol{\theta}_{n-1} \hat{\boldsymbol{\phi}}_n \right) \mathbf{X} + \mathcal{O}(\epsilon^2) \\ &= \mathbf{Y} + \epsilon \sum_{i=1}^n \left(\boldsymbol{\theta}_1 \cdots \boldsymbol{\theta}_{i-1} \hat{\boldsymbol{\phi}}_i \boldsymbol{\theta}_{i+1} \cdots \boldsymbol{\theta}_n \right) \mathbf{X}.\end{aligned}$$

Taking the norm, we obtain,

$$\|\bar{\mathbf{Y}} - \mathbf{Y}\| = \epsilon \left\| \sum_{i=1}^n \left(\boldsymbol{\theta}_1 \cdots \boldsymbol{\theta}_{i-1} \hat{\boldsymbol{\phi}}_i \boldsymbol{\theta}_{i+1} \cdots \boldsymbol{\theta}_n \right) \right\| \|\mathbf{X}\|.$$

Therefore,

$$\frac{\|\bar{\mathbf{Y}} - \mathbf{Y}\|}{\|\mathbf{X}\|} = \epsilon \left\| \sum_{i=1}^n \left(\boldsymbol{\theta}_1 \cdots \boldsymbol{\theta}_{i-1} \hat{\boldsymbol{\phi}}_i \boldsymbol{\theta}_{i+1} \cdots \boldsymbol{\theta}_n \right) \right\|.$$

This expression shows that for an input \mathbf{X} , the output shift is directly proportional to the sample scaling factor ϵ . ■

Lemma 5 *The final model output estimated by MonteCLoRA is an unbiased estimator of the original model output.*

Proof An important conclusion from the parameterization shown in the previous section is the expected value of $\bar{\mathbf{Y}}$. Since each weight matrix is assumed to be independent, we have,

$$\begin{aligned}\mathbb{E}[\bar{\mathbf{Y}}] &= \mathbb{E} \left[(\boldsymbol{\theta}_1 + \epsilon \hat{\boldsymbol{\phi}}_1) \right] \mathbb{E} \left[(\boldsymbol{\theta}_2 + \epsilon \hat{\boldsymbol{\phi}}_2) \right] \cdots \mathbb{E} \left[(\boldsymbol{\theta}_n + \epsilon \hat{\boldsymbol{\phi}}_n) \right] \mathbf{X} \\ \mathbb{E}[\bar{\mathbf{Y}}] &= (\boldsymbol{\theta}_1 + \epsilon \mathbb{E}[\hat{\boldsymbol{\phi}}_1]) (\boldsymbol{\theta}_2 + \epsilon \mathbb{E}[\hat{\boldsymbol{\phi}}_2]) \cdots (\boldsymbol{\theta}_n + \epsilon \mathbb{E}[\hat{\boldsymbol{\phi}}_n]) \mathbf{X}\end{aligned}$$

Since each $\hat{\boldsymbol{\phi}}_i$ is a weighted sum of samples from a Gaussian distribution with zero mean, we have $\mathbb{E}[\hat{\boldsymbol{\phi}}_i] = 0$. Therefore,

$$\mathbb{E}[\bar{\mathbf{Y}}] = \boldsymbol{\theta}_1 \boldsymbol{\theta}_2 \cdots \boldsymbol{\theta}_n \mathbf{X} = \mathbf{Y}.$$
■

Hence, in expectation, the model's prediction is not dependent on the sample scaler. This property is beneficial during inference. We run the model at inference time like the standard LoRA model, utilizing the fine-tuned weights guided by MonteCLoRA enhancements. As a result, inference times remain the same because we do not need to perform sampling during inference.

Lemma 6 *The estimator described in Equation 18 is an unbiased estimator for the expected posterior defined in Equation 17.*

Proof Let $\hat{\theta}_i$ denote the estimator in Equation 18. To show that the Monte Carlo estimator is an unbiased estimator of the true expectation, we compute $\mathbb{E}[\hat{\theta}_i]$ and demonstrate that it equals $\mathbb{E}[\theta_i]$. For fixed $\mathbf{\Pi}^{(j)}$ and $\mathbf{\Sigma}^{(j)}$, the expectation of $\frac{1}{N} \sum_{k=1}^N \theta_i^{(k,j)}$ over the samples $\theta_i^{(k,j)}$ is,

$$\mathbb{E} \left[\frac{1}{N} \sum_{k=1}^N \theta_i^{(k,j)} \mid \mathbf{\Pi}^{(j)}, \mathbf{\Sigma}^{(j)} \right] = \mathbb{E}[\theta_i \mid \mathbf{\Pi}^{(j)}, \mathbf{\Sigma}^{(j)}].$$

By the law of large numbers, as $N \rightarrow \infty$, the sample mean $\frac{1}{N} \sum_{i=k}^N \theta_i^{(k,j)}$ converges to the conditional expectation $\mathbb{E}[\theta_i \mid \mathbf{\Pi}^{(j)}, \mathbf{\Sigma}^{(j)}]$. Next, we consider the expectation of the outer sum over the samples $\mathbf{\Pi}^{(j)}$ and $\mathbf{\Sigma}^{(j)}$ as,

$$\mathbb{E} \left[\frac{1}{M} \sum_{j=1}^M \mathbb{E}[\theta_i \mid \mathbf{\Pi}^{(j)}, \mathbf{\Sigma}^{(j)}] \right] = \mathbb{E}_{\mathbf{\Pi}, \mathbf{\Sigma}}[\mathbb{E}[\theta_i \mid \mathbf{\Pi}, \mathbf{\Sigma}]].$$

Using the law of total expectation, we have

$$\mathbb{E}_{\mathbf{\Pi}, \mathbf{\Sigma}}[\mathbb{E}[\theta_i \mid \mathbf{\Pi}, \mathbf{\Sigma}]] = \mathbb{E}[\theta_i].$$

Therefore, as $M \rightarrow \infty$, the outer sum $\frac{1}{M} \sum_{j=1}^M \mathbb{E}[\theta_i \mid \mathbf{\Pi}^{(j)}, \mathbf{\Sigma}^{(j)}]$ converges to $\mathbb{E}[\theta_i]$, which is the original integral. Hence, in expectation, the Monte Carlo estimator $\hat{\theta}_i$ converges to the true integral $\mathbb{E}[\hat{\theta}_i] = \mathbb{E}[\theta_i]$. This demonstrates that, given sufficiently large N and M , the Monte Carlo estimate will approximate the desired expectation $\mathbb{E}[\theta_i]$. \blacksquare

Lemma 7 *The estimator described in Equation 18 is a robust estimator for the integral in Equation 17.*

Proof To find the covariance of the Monte Carlo estimator described in Equation 18, we need to analyze both the inner and outer layers of sampling over θ_i , $\mathbf{\Pi}$, and $\mathbf{\Sigma}$. The variance of this estimator will depend on the variability from both layers. We first decompose the covariance using the law of total covariance; we can decompose the variance of $\hat{\theta}_i$ as follows,

$$\text{Cov}(\hat{\theta}_i) = \mathbb{E}_{\mathbf{\Pi}, \mathbf{\Sigma}} \left[\text{Cov}_{\theta_i} \left(\frac{1}{N} \sum_{k=1}^N \theta_i^{(k,j)} \mid \mathbf{\Pi}, \mathbf{\Sigma} \right) \right] + \text{Cov}_{\mathbf{\Pi}, \mathbf{\Sigma}} \left(\mathbb{E}_{\theta_i} \left[\frac{1}{N} \sum_{k=1}^N \theta_i^{(k,j)} \mid \mathbf{\Pi}, \mathbf{\Sigma} \right] \right).$$

- The first term, $\mathbb{E}_{\mathbf{\Pi}, \mathbf{\Sigma}} \left[\text{Cov}_{\theta_i} \left(\frac{1}{N} \sum_{i=1}^N \theta_i^{(i,j)} \mid \mathbf{\Pi}, \mathbf{\Sigma} \right) \right]$, represents the expected conditional covariance given $\mathbf{\Pi}$ and $\mathbf{\Sigma}$.
- The second term, $\text{Cov}_{\mathbf{\Pi}, \mathbf{\Sigma}} \left(\mathbb{E}_{\theta_i} \left[\frac{1}{N} \sum_{i=1}^N \theta_i^{(i,j)} \mid \mathbf{\Pi}, \mathbf{\Sigma} \right] \right)$, represents the covariance due to the variability in $\mathbf{\Pi}$ and $\mathbf{\Sigma}$.

For fixed $\mathbf{\Pi}$ and $\mathbf{\Sigma}$, the covariance of the average $\frac{1}{N} \sum_{k=1}^N \theta_i^{(k,j)}$ is,

$$\text{Cov}_{\theta_i} \left(\frac{1}{N} \sum_{k=1}^N \theta_i^{(k,j)} \mid \mathbf{\Pi}, \mathbf{\Sigma} \right) = \frac{1}{N} \text{Cov}_{\theta_i}(\theta_i \mid \mathbf{\Pi}, \mathbf{\Sigma}),$$

where $\text{Cov}_{\theta_i}(\boldsymbol{\theta}_i | \boldsymbol{\Pi}, \boldsymbol{\Sigma})$ is the conditional covariance of $\boldsymbol{\theta}_i$ given $\boldsymbol{\Pi}$ and $\boldsymbol{\Sigma}$. So, the first term becomes,

$$\mathbb{E}_{\boldsymbol{\Pi}, \boldsymbol{\Sigma}} \left[\frac{1}{N} \text{Cov}(\boldsymbol{\theta}_i | \boldsymbol{\Pi}, \boldsymbol{\Sigma}) \right] = \frac{1}{N} \mathbb{E}_{\boldsymbol{\Pi}, \boldsymbol{\Sigma}} [\text{Cov}_{\theta_i}(\boldsymbol{\theta}_i | \boldsymbol{\Pi}, \boldsymbol{\Sigma})].$$

The conditional covariance can be computed as,

$$\text{Cov}(\boldsymbol{\theta} | \boldsymbol{\Pi}, \boldsymbol{\Sigma}) = \sum_i \pi_i^2 \boldsymbol{\Sigma}.$$

On taking expectation over $\boldsymbol{\Pi}$ and $\boldsymbol{\Sigma}$, we obtain,

$$\frac{1}{N} \mathbb{E}_{\boldsymbol{\Pi}, \boldsymbol{\Sigma}} \left[\sum_i \pi_i^2 \boldsymbol{\Sigma} \right] = \frac{1}{N} \sum_i \mathbb{E}_{\boldsymbol{\Pi}} [\pi_i^2] \boldsymbol{\Sigma} = \frac{\boldsymbol{\Sigma}}{N} \sum_i \mathbb{E}_{\boldsymbol{\Pi}} [\pi_i^2].$$

The second term in the covariance decomposition accounts for the variability of the conditional expectation $\mathbb{E}[\boldsymbol{\theta} | \boldsymbol{\Pi}, \boldsymbol{\Sigma}]$ due to the sampling of $\boldsymbol{\Pi}$ and $\boldsymbol{\Sigma}$. We can write this term as,

$$\text{Cov}_{\boldsymbol{\Pi}, \boldsymbol{\Sigma}} (\mathbb{E}[\boldsymbol{\theta} | \boldsymbol{\Pi}, \boldsymbol{\Sigma}]) = \frac{1}{M} \text{Cov}_{\boldsymbol{\Pi}, \boldsymbol{\Sigma}} (\mathbb{E}[\boldsymbol{\theta} | \boldsymbol{\Pi}, \boldsymbol{\Sigma}]).$$

The expectation of $\boldsymbol{\theta}$ given $\boldsymbol{\Pi}$ and $\boldsymbol{\Sigma}$ is just the mean of the distribution, which is independent of $\boldsymbol{\Pi}$ and $\boldsymbol{\Sigma}$. Hence the second term goes to zero. Putting it all together, the covariance of the estimator $\hat{\boldsymbol{\theta}}_i$ is,

$$\text{Cov}(\hat{\boldsymbol{\theta}}_i) = \frac{\boldsymbol{\Sigma}}{N} \mathbb{E}_{\boldsymbol{\Pi}} \left[\sum_i \pi_i^2 \right].$$

Therefore, as $N \rightarrow \infty$, the covariance reduces, making the estimator robust. ■

Lemma 8 *Training a model with Gaussian noise added to parameters is less sensitive to learning rates.*

Proof Let the model parameters be denoted by $\boldsymbol{\theta}$, and the Gaussian noise added to these parameters by $\boldsymbol{\gamma}$. The learning rates of the model with and without Gaussian noise are represented as $\tilde{\eta}$ and η , respectively, and the corresponding Lipschitz constants are \tilde{L} and L . The remaining notations follow from the previous lemmas. From Lemma 3, we know that for all $\boldsymbol{\theta} \in \mathbb{R}^N$, the maximum eigenvalue of the Hessian of the smoothed loss function satisfies,

$$\lambda_{\max}(\tilde{H}(\boldsymbol{\theta})) \leq \Lambda_{\max}.$$

Taking the supremum over all $\boldsymbol{\theta}$ and using the properties of the supremum, we obtain

$$\tilde{\Lambda}_{\max} \leq \Lambda_{\max},$$

where Λ_{\max} represents the supremum of the maximum eigenvalues of the Hessian of the original loss function $J(\boldsymbol{\theta})$, and $\tilde{\Lambda}_{\max}$ is the supremum of the maximum eigenvalues of

the expected Hessian of the smoothed loss function $\tilde{J}(\boldsymbol{\theta})$. From Lemma 2, we have the relationship between the Lipschitz constants and the supremum of the Hessian eigenvalues,

$$L = \Lambda_{\max} \quad \text{and} \quad \tilde{L} = \tilde{\Lambda}_{\max}.$$

Therefore, we conclude

$$\tilde{L} \leq L.$$

Since $\tilde{L} \leq L$, and we know that the range of learning rates on which we can guarantee convergence is inversely proportional to the Lipschitz constant, we can say that training with Gaussian noise permits a broader range of allowable learning rates, thus reducing sensitivity to the choice of learning rate during optimization. \blacksquare

4.4 Training Objectives

4.4.1 REPARAMETERIZATION LOSSES

We incorporate a series of Kullback-Leibler divergence (KLD) losses into the objective function to regularize the learned prior distributions. These losses are crucial for shaping the model’s latent weight space and preventing overfitting. For each sampling process within the model, a corresponding KLD loss is added. The sum of all these KLD losses across layers is scaled by a KL divergence weight parameter η and incorporated into the final loss.²

- **Multivariate Gaussian KL Divergence Loss.** In MonteCLoRA, the distribution to be optimized is a multivariate Gaussian distribution with parameters $(\boldsymbol{\mu}, \hat{\boldsymbol{\Sigma}})$ and it is optimized against a multivariate Gaussian with parameters $(\boldsymbol{\mu}, \mathbf{I})$. We refer to the distribution to be optimized as P and the standard normal as Q . The KL divergence loss can be computed as,

$$\text{KL}_{\mathcal{N}} = \frac{1}{2} \left(\text{tr}(\hat{\boldsymbol{\Sigma}}) - \ln |\hat{\boldsymbol{\Sigma}}| - n_{\text{out}} \right). \quad (19)$$

- **Wishart KL Divergence Loss.** We optimise the Wishart Distribution of MonteCLoRA, $\mathcal{W}_{n_{\text{out}}}(\mathbf{V}, n_{\text{in}})$, against the standard Wishart distribution, $\mathcal{W}_{n_{\text{out}}}(\mathbf{I}, n_{\text{in}})$. We keep the degree of freedom and dimensionality the same to focus on optimizing the scale matrix. We refer to the distribution to be optimized as P and the standard distribution as Q . The KL divergence can be calculated in closed form as,

$$\text{KL}_{\mathcal{W}} = \frac{1}{2} (n_{\text{in}} (-\ln |\mathbf{V}|) + n_{\text{in}}, \text{tr}(\mathbf{V}) - n_{\text{in}}n_{\text{out}}). \quad (20)$$

- **Dirichlet KL Divergence Loss.** We have N -Dimensional Dirichlet random vectors following the distributions (P and Q) with parameters $\boldsymbol{\alpha}_1$ and $\boldsymbol{\alpha}_2$, respectively, where

2. Derivation of the KL divergence losses are furnished in the Appendix A.3.

$\alpha_1, \alpha_2 \in \mathbb{R}^N$. In **MonteCLoRA**, we take α_2 as a constant vector with all the same values. The KL divergence of P from Q is given by,

$$\text{KL}_{\mathcal{D}} = \ln \frac{\Gamma\left(\sum_{i=1}^N \alpha_{1i}\right)}{\Gamma\left(\sum_{i=1}^N \alpha_{2i}\right)} + \sum_{i=1}^N \ln \frac{\Gamma(\alpha_{2i})}{\Gamma(\alpha_{1i})} + \sum_{i=1}^N (\alpha_{1i} - \alpha_{2i}) \left[\psi(\alpha_{1i}) - \psi\left(\sum_{j=1}^N \alpha_{1j}\right) \right]. \quad (21)$$

Here, Γ is the gamma, and ψ is the digamma (logarithmic derivative of gamma) function.

4.4.2 COOPERATIVE LOSS

To ensure maximal participation from each of the N mixture component, we compute a *cooperative loss*. For mixture weights $\pi_1, \pi_2, \dots, \pi_N$ obtained from the Dirichlet samples, the cooperative loss is calculated as $\sum_{i=1}^N \pi_i^2$. To promote higher cooperation, we minimize the cooperative loss,

$$\mathcal{L}_{\mathcal{C}} = \sum_{i=1}^N \pi_i^2. \quad (22)$$

Lemma 9 *Cooperative loss defined in Equation 22 is minimized when $\pi_i = \frac{1}{N} \forall i \in [1, N]$.*

Proof Using the fact $\sum_{i=1}^N \pi_i = 1$, we can rewrite $\mathcal{L}_{\mathcal{C}}$ as,

$$\pi_1^2 + \pi_2^2 + \dots + (1 - \sum_{i=1}^{N-1} \pi_i)^2 = 1 + 2 \sum_{i=1}^{N-1} \pi_i^2 - 2 \sum_{i=1}^{N-1} \pi_i + 2 \sum_{i=1}^{N-1} \sum_{j \neq i} \pi_i \pi_j.$$

Therefore, for $\frac{\partial \mathcal{L}_{\mathcal{C}}}{\partial \pi_i} = 0$, we get,

$$\begin{aligned} 4\pi_i - 2 + 2 \sum_{j \neq i} \pi_j &= 0 \\ \implies 2\pi_i &= 2 - 2 \sum_{i=1}^{N-1} \pi_i \\ \implies 2\pi_i &= 2\pi_N. \end{aligned}$$

Hence, $\pi_1 = \pi_2 = \dots = \pi_N = \frac{1}{N}$. As $\frac{\partial^2 \mathcal{L}_{\mathcal{C}}}{\partial^2 \pi_i} = 4 > 0$, $\frac{1}{N}$ is the minima. ■

4.4.3 FINAL LOSS FUNCTION

Combining all the training objectives, the final loss function can be defined as,

$$\mathcal{L} = \sum_{(x,y) \in Z} \sum_{t=1}^{|y|} \log P_{\Phi_0 + \Delta \Phi(\Theta, \zeta)}(y_t | x, y_{<t}) + \eta \cdot \frac{(\text{KL}_{\mathcal{D}} + \text{KL}_{\mathcal{W}} + \text{KL}_{\mathcal{N}})}{N_{\text{MonteCLoRA}}} + \mathcal{L}_{\mathcal{C}}.$$

Here, $N_{\text{MonteCLoRA}}$ denotes the total number of **MonteCLoRA** layers. The division by $N_{\text{MonteCLoRA}}$ and the KLD loss weight η serve to normalize and scale down the contribution of the KL divergence losses, ensuring balanced training dynamics.

5 Experiments

5.1 Datasets and Tasks

To evaluate the effectiveness of `MonteCLoRA`, we conduct thorough empirical study across two different ranges of tasks – natural language understanding (NLU) and natural language generation (NLG).

For NLU, we use five tasks from the GLUE (Wang et al., 2018) and SuperGLUE (Wang et al., 2019) benchmarks, namely MRPC (Dolan and Brockett, 2005), CoLA (Warstadt et al., 2019), RTE (Dagan et al., 2005; Haim et al., 2006; Giampiccolo et al., 2007; Ben-tivogli et al., 2009), WiC (Pilehvar and Camacho-Collados, 2018) and BoolQ (Clark et al., 2019). Details of these datasets can be found in Appendix A.1. These gold standard datasets for these tasks contain separate train and dev (also called validation) split, where we use the train dataset to fine-tune LLMs and dev dataset for evaluation. For these tasks, we consider the intrinsic evaluation metric – negative loglikelihood (NLL) and extrinsic evaluation metric – accuracy. On NLG, we consider six commonsense reasoning tasks – PiQA (Bisk et al., 2020), Social (Sap et al., 2019), WinoGrande (Sakaguchi et al., 2021), ARC-easy, ARC-challenge (Clark et al., 2018) and OpenBookQA (Mihaylov et al., 2018). Details of these tasks are mentioned in Appendix A.1. For these tasks, we use the Commonsense15K dataset (Hu et al., 2023). This dataset is particularly curated for instruction fine-tuning of LLMs and comprises of subsets of training samples from different commonsense reasoning tasks. The final output for these NLG tasks contains the answer to a multiple-choice question and is evaluated using accuracy.

5.2 Models

For NLU, we use a pre-trained RoBERTA-base (Liu et al., 2019) (110M parameters) model. For generative tasks, we use the pre-trained LLaMA-1-7B (Touvron et al., 2023) model. All the pre-trained model weights are obtained from Huggingface (Wolf et al., 2020).

5.3 Baselines

Apart from full fine-tuning and LoRA (Hu et al., 2022) fine-tuning strategies, we compare the performance of `MonteCLoRA` against the competitive parameter-efficient fine-tuning methods.

- **AdaLoRA.** Zhang et al. (2023) improved upon vanilla LoRA by dynamically adjusting the ranks of the rank-decomposition matrices, facilitating the allocation of more capacity to important weights and reducing it for less significant ones.
- **DoRA.** Liu et al. (2024) improved on LoRA by decomposing the pre-trained weight into two components, magnitude and direction, for fine-tuning. By employing LoRA for directional updates to efficiently minimize the number of trainable parameters, DoRA makes sure to enhance the learning capacity and training stability of LoRA while avoiding any additional inference overhead.
- **Laplace LoRA.** Yang et al. (2024) brought a Bayesian approach to LoRA by applying a Laplace approximation to the posterior over LoRA parameters to overcome uncertainty and overconfidence and ensure better model calibration.

Type	Hyperparameter	RoBERTa-base	LLaMA-1-7B
Static	LoRA r	8	32
	LoRA α	16	64
	Max Sequence Length	256	256
	Learning Rate Scheduler	Linear	Linear
	Epochs	20	3
Tunable	Batch Size	{8, 32, 64}	{8, 16, 32}
	Learning Rate	$\{3 \times 10^{-4}, 5 \times 10^{-5}, 1 \times 10^{-5}\}$	$\{3 \times 10^{-4}, 3 \times 10^{-5}\}$

Table 3: Static and tunable hyperparameters used in fine-tuning RoBERTa-base and LLaMA-1-7B models.

Hyperparameter	Value
Sample Scaler (ϵ)	5×10^{-3}
KL Loss Weight (η)	1×10^{-5}
Dirichlet Prior (α)	1
Mixture Components (N)	4

Table 4: Hyperparameters used for MonteCLoRA.

5.4 Hyperparameters

As described in Section 1, LLM fine-tuning strategies are very sensitive to hyperparameters. For the reproducibility of our study, we describe the hyperparameters used in MonteCLoRA and the baseline on different tasks. Table 3 contains the static and tunable hyperparameters used for all the fine-tuning methods with RoBERTa and LLaMA models. Static hyperparameters are used for all the model-specific training tasks and are the same for all the fine-tuning strategies. We tune the optimizer learning rate and the training batch size for the robustness studies for different strategies. Table 4 reports the hyperparameters specific to MonteCLoRA. The hyperparameters are the default ones used in our method and are used in all the NLU and NLG tasks. In the subsequent sections, we discuss the importance of these hyperparameters in greater detail. All our experiments were conducted on NVIDIA A100-80GB GPUs that had access to the CUDA 12.5 environment.

6 Experimental Results

In this section, we discuss the results obtained from the empirical study with the NLU and NLG tasks.

6.1 Evaluation on NLU Tasks

Figure 4 highlights the distribution of accuracy (extrinsic metric) and negative loglikelihood (intrinsic metric) calculated on the validation dataset of the GLUE and SuperGLUE tasks with the RoBERTa-base model. We compare MonteCLoRA with full fine-tuning (denoted as Full FT), LoRA and AdaLoRA. The distribution spread is highest in case of full fine-tuning, with the average spread being 0.15 and 19.61, respectively, on the intrinsic and extrinsic metrics. Although the inter-quartile range (IQR) remains modest for most tasks, the spread in accuracy is noticeably large on most tasks. This observation underscores that fully fine-

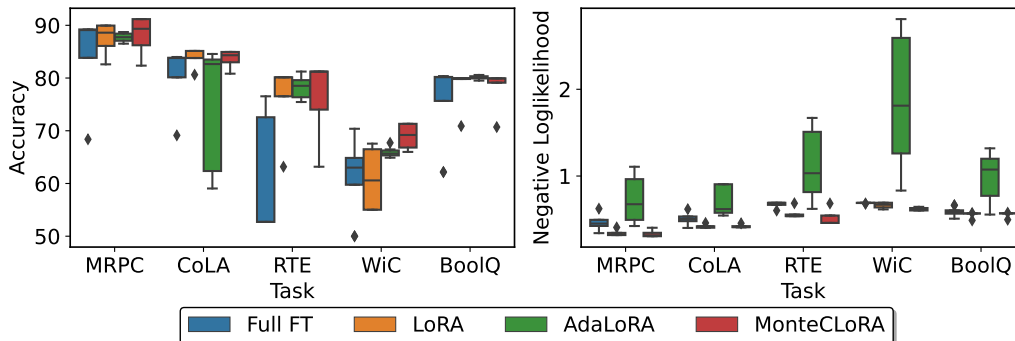


Figure 4: Distribution of accuracies and negative loglikelihood of RoBERTa-base on different GLUE tasks with different fine-tuning strategies.

Method	Robustness	MRPC	CoLA	RTE	WiC	BoolQ	Average
Full FT		2.21	1.98	1.45	1.45	1.71	1.76
LoRA	Intrinsic \uparrow	3.11	2.38	1.86	1.49	1.76	2.12
AdaLoRA		1.48	1.61	0.97	0.55	0.93	1.10
MonteCLoRA		3.16	2.43	2.18	1.63	1.75	2.23
Full FT		89.1	83.8	52.7	63.0	80.1	73.7
LoRA	Extrinsic \uparrow	88.6	83.8	80.1	60.6	80.0	78.6
AdaLoRA		87.7	82.6	78.5	65.7	80.2	79.0
MonteCLoRA		89.3	84.3	81.2	69.2	79.9	80.8

Table 5: Robustness of different fine-tuning strategies with RoBERTa-base on GLUE and SuperGLUE tasks. We underline the tasks where MonteCLoRA achieves higher robustness score than LoRA fine-tuning.

tuning LLMs can be prone to under-generalization, where the performance on the validation dataset could be abysmally low. Among the low-rank adaptation methods, AdaLoRA has the highest spread of 0.96 with the intrinsic metric, which highlights the inability to calibrate output confidence under different hyperparameter configurations. LoRA has a low spread of 0.09 with NLL, same as MonteCLoRA. However, the spread with accuracy distribution is one point higher with LoRA than MonteCLoRA. On smaller tasks like WiC, LoRA demonstrates a 7 points higher spread than MonteCLoRA. MonteCLoRA shows higher stability in terms of both metrics, justifying its effectiveness in maintaining stability in performance and confidence in its predictions.

Table 5 shows the intrinsic and extrinsic robustness defined in Section 3.3 for different fine-tuning methods. The above discussion confirms that MonteCLoRA tends to have less probability of outliers with intrinsic or extrinsic metrics. The robustness metrics highlight the method’s stability in terms of maintaining the probability of having good performance. We observe the highest average intrinsic robustness value of 2.23 with MonteCLoRA, which is 5% higher than that of LoRA. AdaLoRA demonstrates the lowest intrinsic robustness, 51% lower than MonteCLoRA. MonteCLoRA also exhibits the highest extrinsic robustness of 80.8, which is 2.2 points higher than LoRA. We perform Wilcoxon signed-rank test to statistically validate whether MonteCLoRA is more robust than the other baselines. The rank tests conclude that MonteCLoRA is more robust than LoRA and its variants, in terms of both intrinsic

Method	Metric	MRPC	CoLA	RTE	WiC	BoolQ	Average
Full FT		89.2	84.0	76.5	70.4	80.4	80.1
LoRA	Accuracy \uparrow	89.9	85.1	80.1	67.5	80.0	80.5
AdaLoRA		88.7	84.5	81.2	67.7	80.6	80.5
MonteCLOrA		91.2	84.9	81.2	71.3	79.9	81.7
Full FT		0.34	0.40	0.60	0.68	0.51	0.51
LoRA	NLL \downarrow	0.32	0.40	0.54	0.62	0.49	0.47
AdaLoRA		0.42	0.54	0.62	0.83	0.55	0.59
MonteCLOrA		0.31	0.41	0.46	0.60	0.50	0.46

Table 6: Comparison of different fine-tuning strategies with RoBERTa-base on GLUE and SuperGLUE tasks. We report the highest accuracy and lowest negative loglikelihood (NLL) obtained across different hyperparameter configurations. The best strategy is highlighted in **bold** for each task.

Metric	Method	MRPC	CoLA	RTE	WiC	BoolQ	Average
Accuracy \uparrow	MonteCLOrA (best)	91.2	84.9	81.2	71.3	79.9	81.7
	MonteCLOrA (median)	89.3	84.3	81.2	69.2	79.9	80.8
	MAP	86.4	81.8	70.9	63.9	77.2	76.0
	MC Dropout (Gal and Ghahramani, 2016)	87.1	82.6	72.4	68.8	76.6	77.5
	Checkpoint Ensemble (Chen et al., 2017)	86.3	81.4	71.8	64.7	77.2	76.3
	Temp (Guo et al., 2017)	86.5	81.8	72.6	65.4	77.3	76.7
	LLLA (Yang et al., 2024)	86.4	81.8	72.6	65.3	77.4	76.7
	LA (Yang et al., 2024)	86.4	81.7	72.6	65.4	77.4	76.7
NLL \downarrow	MonteCLOrA (best)	0.31	0.41	0.46	0.60	0.50	0.46
	MonteCLOrA (median)	0.32	0.41	0.46	0.61	0.57	0.47
	MAP	0.66	0.50	0.76	1.00	0.54	0.69
	MC Dropout (Gal and Ghahramani, 2016)	0.39	0.39	0.58	0.72	0.50	0.52
	Checkpoint Ensemble (Chen et al., 2017)	0.44	0.49	0.57	0.63	0.53	0.53
	Temp (Guo et al., 2017)	0.32	0.40	0.54	0.62	0.49	0.47
	LLLA (Yang et al., 2024)	0.33	0.44	0.56	0.78	0.51	0.52
	LA (Yang et al., 2024)	0.34	0.39	0.54	0.62	0.48	0.47

Table 7: Comparison of different Bayesian post-hoc methods applied to pre-trained RoBERTa-base model and LoRA fine-tuning on various GLUE and SuperGLUE tasks. Results of baselines apart from MonteCLOrA are obtained from Yang et al. (2024). The bold results indicate the cases where MonteCLOrA performs better than the other Bayesian baselines.

(p -value $0.06 < 0.1$) and extrinsic (p -value $0.09 < 0.1$) robustness metrics. Full fine-tuning has the lowest extrinsic robustness of 73.7, indicating its inability to generalize well across different NLU tasks. The underperformance of full fine-tuning also suggests that training the full language model on all downstream tasks is inefficient and could be ineffective for certain tasks. Particularly on tasks like RTE, full fine-tuning can diverge and exhibit very poor performance on validation. Remarkably, MonteCLOrA achieves higher intrinsic and extrinsic robustness than LoRA and its variant in four out of five tasks, emphasizing its ability to showcase robustness across different tasks and training configurations.

Table 6 reports the highest accuracy and the lowest negative loglikelihood (correspondingly, highest loglikelihood) achieved by different fine-tuning methods on NLU tasks. Interestingly, the variance among the baselines is significantly lower when the best results are concerned. On average, the best accuracy obtained with full fine-tuning is 80.1%, which is

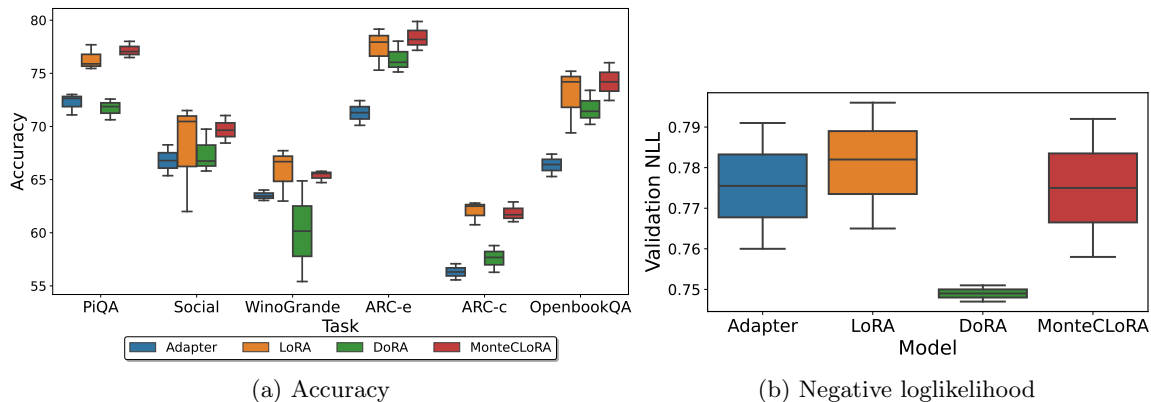


Figure 5: Distribution of test accuracies and validation negative loglikelihood of LLaMA-1-7B on different commonsense reasoning tasks with different fine-tuning strategies.

Method	PiQA	Social	WinoGrande	ARC-e	ARC-c	OpenbookQA	Average
Adapter	73.0	68.3	64.0	72.4	57.1	67.4	67.0
LoRA	77.7	71.5	67.7	79.2	62.8	75.2	72.3
DoRA	72.6	69.7	64.9	78.0	58.8	73.4	69.6
MonteCLoRA	78.0	71.0	65.8	79.9	62.9	76.0	72.3

Table 8: Performance of different fine-tuning strategies with pre-trained LLaMA-1-7B on generative tasks.

only 0.4% lower than LoRA and AdaLoRA. **MonteCLoRA** beats the baselines with a margin of 1.2%, demonstrating its superiority in achieving better performance across different hyperparameter configurations. Remarkably, **MonteCLoRA** beats the current state-of-the-art AdaLoRA on these tasks. It also achieves the lowest NLL among all the baselines, indicating its superiority in generalization across multiple tasks.

We compare **MonteCLoRA** against the contemporary Bayesian post-hoc methods on the NLU tasks in Table 7. The Bayesian methods such as maximum a-posteriori (MAP), Monte Carlo dropout (MC Dropout), and Laplace-LoRA (LA) offer flexible solutions to applying Bayesian treatment to LoRA fine-tuning in a post-hoc manner (i.e., can be used after the LoRA method is trained). Our comparative analysis suggests that **MonteCLoRA** can perform better than the existing Bayesian post-hoc methods with fewer training steps. As argued by Yang et al. (2024), these methods require longer training steps for calibrating output probabilities generated in the fine-tuning phase. Even when we consider the median performance of **MonteCLoRA**, it still achieves 3.2% higher accuracy than the best baseline, Monte Carlo Dropout. In terms of the negative loglikelihood, **MonteCLoRA** achieves the best performance among all these Bayesian post-hoc methodologies.

6.2 Evaluation on NLG Tasks

We follow a similar empirical study for the generative tasks as in the NLU tasks. Figure 5 highlights the distribution of test accuracy and the validation NLL scores. Contrarily to the NLU tasks, the generative experiments are more intriguing as the extrinsic metrics are

Method	PiQA	Social	WinoGrande	ARC-e	ARC-c	OpenbookQA	Average
Adapter	72.6	66.8	63.4	71.3	56.3	66.4	66.1
LoRA	75.9	70.5	66.7	77.9	62.5	74.2	71.3
DoRA	71.9	66.7	60.1	76.0	57.7	71.4	67.3
MonteCLoRA	77.0	69.6	65.6	78.2	61.7	74.3	71.1

Table 9: Extrinsic robustness of different fine-tuning strategies with LLaMA-1-7B on zero-shot generative tasks.

calculated on a test dataset in a zero-shot manner, i.e., the model might not be aware of the test data distribution during the fine-tuning phase. In terms of the intrinsic metric (NLL), DoRA has the tiniest spread of 0.004 points, whereas both LoRA and MonteCLoRA have a modest spread of 0.03. However, with extrinsic metric, the spread with MonteCLoRA is only 2.2, significantly lower than LoRA (4.6) and DoRA (4.0). Remarkably, on tasks like WinoGrande, the spread with DoRA and LoRA can be as large as 9.5; however, with MonteCLoRA, the spread remains meagre for all the tasks, ensuring higher stability.

In Table 8, we report best accuracies achieved by the different fine-tuning methods on generative tasks. We observe that MonteCLoRA and LoRA exhibit a similar performance on the zero-shot generative tasks. The average accuracies obtained with MonteCLoRA and LoRA remains 72.3, higher than Adapter and DoRA. Out of six tasks, on three tasks, MonteCLoRA achieves better accuracy than LoRA. Out of the remaining three tasks, only in WinoGrande, the margin between LoRA and MonteCLoRA is significant. LoRA and MonteCLoRA are marginally similar for the remaining two tasks. In terms of the robustness metrics (c.f. Table 9), LoRA performs slightly better than MonteCLoRA. Particularly on ARC-challenge and WinoGrande, LoRA achieves ~ 1 point better robustness than MonteCLoRA. However, it is worth noting that the long-tail nature of the accuracy distribution of LoRA makes these results less reliable and less robust. On the other hand, MonteCLoRA balances good performance with excellent stability, overmining its effectiveness in robust fine-tuning.

6.3 Ablation Study

We study the importance of different components of MonteCLoRA with thorough ablation analysis. We use the NLU tasks with the RoBERTa-base coupled with MonteCLoRA fine-tuning for this study. Figure 6 highlights the performance of MonteCLoRA by changing the hyperparameters, including the number of mixture components (N), Dirichlet concentration parameter (α), sample scaler (ϵ), KLD loss weight (η), and the importance of cooperative loss defined in Equation 22.

Effect of the Number of Mixture Components. Lemma 7 suggests that MonteCLoRA estimates a robust estimator with a large number of mixture components. However, in Figure 6(a), we observe that MonteCLoRA can achieve robust performance even with only four mixture components. Increasing the mixtures to 16 has very minimal impact on the accuracy and the loglikelihood of the fine-tuned model. Having too less number of mixture components could lead to underfitting, hurting the performance of the fine-tuned model.

Importance of Dirichlet Concentration Initialization. To understand the impact of initialization of the Dirichlet concentration, we perform an ablation where instead of

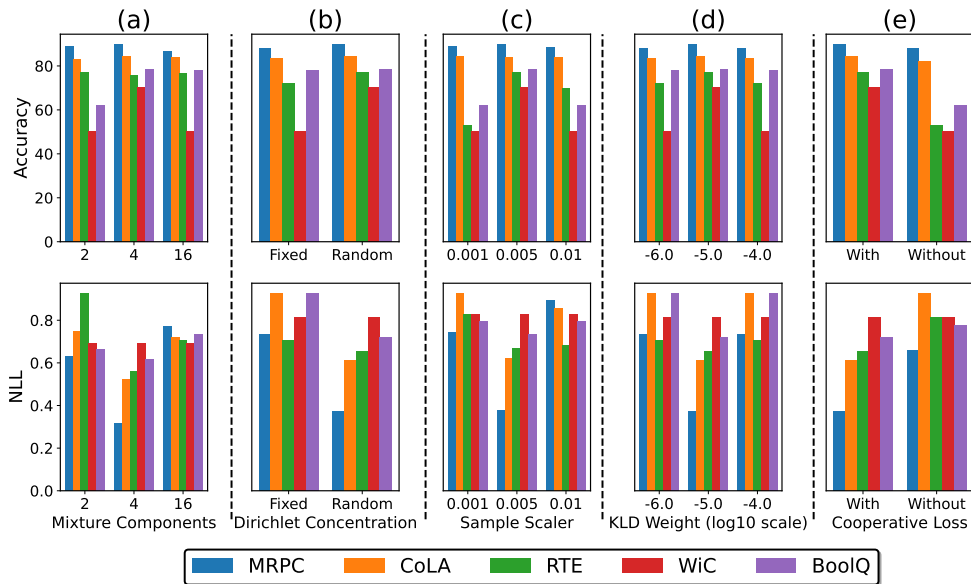


Figure 6: Ablation of MonteCLoRA with RoBERTa-base on different GLUE tasks with respect to (a) the number of mixture components N , (b) Dirichlet concentration parameter α , (c) Sample scaler ϵ , (d) KLD weight (η), and (e) cooperative loss.

initializing the value with $\alpha = 1$, we use a random vector $\mathcal{U}(0, 1)^N$, where \mathcal{U} is a uniform distribution. We call this ablation ‘random’ Dirichlet concentration. The results are particularly surprising (c.f. Figure 6(b)), where we observe an average $> 2\%$ improvement in accuracy with random initialization. Random prior can improve the accuracy on tasks like RTE by a margin of 4%. Random initialization of Dirichlet concentration parameters allows the model for more exploration, learning the mixture dynamics better.

Sample Scaler and KLD Loss Weight for Balancing Exploration-Exploitation.

In Algorithm 1, we described the importance of the sample scaler ϵ to dynamically control the exploration of different optimization basins of the low-rank parameters. The ablation results in Figure 6(c) highlights an interesting pattern: with a moderate $\epsilon = 0.005$, MonteCLoRA achieves the best validation accuracy. The results emphasize the importance of balancing exploration and exploitation for a stable convergence of the fine-tuned model. In RTE, WiC, and BoolQ, a high ϵ can diverge the model, whereas a low ϵ can lead to overfitting the training data, both impacting the validation performance. A similar observation is found with the KLD loss weight (η) in Figure 6(d). A high KLD loss weight indicates more regularization towards the prior distributions, whereas a low KLD loss weight indicates assigning more importance to the likelihood term, relaxing the prior conditions. Having a moderate $\eta = 10^{-5}$ leads to better and more stable performance. In fact, $\eta = 10^{-6}$ or $\eta = 10^{-4}$ leads to almost same performance drop of 1% – 4%, for different tasks.

Cooperative Loss for Better Allocation of Mixture Importance. Another critical component of MonteCLoRA training is the cooperative loss. Without cooperative loss, the mixture importance values remain unconstrained and independent. A sense of coop-

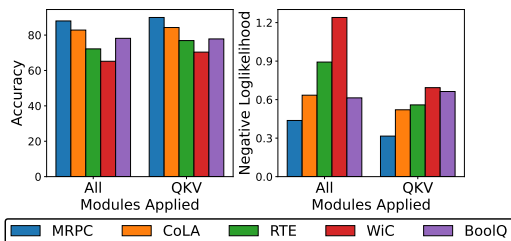


Figure 7: Performance of MonteCLoRA at different modules of RoBERTa-base.

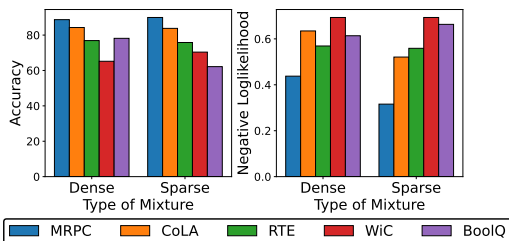


Figure 8: importance of a mixture of samples in MonteCLoRA.

eration between different mixture components ensures that the dynamics of the complex low-rank parameterization is captured. Moreover, with cooperative loss, the importance of different mixture components can be allocated proportionately, maintaining the system’s entropy. In Figure 6(e), we see a drastic $> 3\%$ performance drop without the cooperative loss component, indicating its importance in achieving good generalization.

Flexibility of MonteCLoRA on Different LLM Components. Figure 7 shows the difference in performance on GLUE tasks when MonteCLoRA is applied on all the parameters (including attention query, attention key, attention value, attention output, intermediate output and layer output modules) versus when applied only on attention parameters (query, key and value parameters). The analysis strikes an interesting pattern where we see improvement in performance for larger tasks and marginal performance drop for smaller tasks when MonteCLoRA is applied to all parameters. In larger tasks like BoolQ, applying MonteCLoRA on all parameters improves the negative loglikelihood and accuracy by 0.5 and 0.3 points, respectively. However, on smaller tasks, enabling MonteCLoRA to only attention parameters improves accuracy by a margin of 2% on average. This phenomenon can be justified using the fact that Transformer MLP (which includes the intermediate and layer output modules) blocks encourage sparse activation (Li et al., 2022); therefore, having dense mixtures can adversely affect the fine-tuned model. Moreover, sparse connections are more important on smaller tasks, where overfitting could be a key issue. Therefore, the dense mixture introduced by MonteCLoRA is not particularly effective with MLP blocks, specifically when applied to smaller downstream tasks.

Introducing Sparsity in MonteCLoRA. The previous analysis highlights that a sparser mixture of Gaussian components could be deemed important while fine-tuning LLMs on smaller tasks. To encourage sparsity in the mixture components, we perform an ablation experiment where we choose only one component. Formally, given a mixture weights $\{\pi_1, \pi_2, \dots, \pi_N\}$, we only activate the component k , where $k = \arg \max_i \{\pi_i\}$. Therefore, the updated mixture weight values become,

$$\pi'_i = \begin{cases} 1, & \text{if } i = k \\ 0, & \text{otherwise} \end{cases}$$

Figure 8 highlights the results with dense (the default mixture of components) and sparse components on NLU tasks. We observe a significant accuracy improvement on two smaller tasks, MRPC and WiC (1.2% and 5%, respectively) with the sparse mixture. The results

illustrate the flexibility of adapting **MonteCLoRA** on different complexities of tasks, which most existing low-rank parameterization-based fine-tuning methods fail to exhibit.

Post-hoc Abilities of MonteCLoRA. In Section 2, we described the post-hoc Bayesian methods for robust and calibrated reparameterization of fine-tuned LLMs. Therefore, to assess the effectiveness of **MonteCLoRA** in post-hoc execution, we perform experiments where we first fine-tune the LLM with only the μ parameter (defined in Algorithm 1) for 10 epochs and fine-tune the $\mathbf{W}_{\text{stochastic}}$ parameter in the remaining 10 epochs, keeping μ frozen. We refer to this experiment as ‘post-hoc’

MonteCLoRA. Decoupling the training of μ and $\mathbf{W}_{\text{stochastic}}$ has several computational advantages. Post-hoc execution is particularly useful when the LLM is already fine-tuned and requires incremental calibration. On the downside, post-hoc execution might require more careful consideration, as if the fine-tuned model is struck in local optima, it may not be able to come out even after the post-hoc execution. Our observation with post-hoc **MonteCLoRA** in Figure 9 is rather more intriguing, where we observe performance improvement on smaller tasks – WiC (5%) and MRPC (0.7%) and almost similar performance on CoLA and RTE. On BoolQ, RoBERTa trained with **MonteCLoRA** post-hoc diverges due to instability during previous LoRA fine-tuning. However, it is important to note that existing Bayesian post-hoc operations require significant effort to mitigate the calibration and robustness challenges of low-rank fine-tuning. On the other hand, **MonteCLoRA** offers faster convergence (more discussion on this topic in the next section) with more robust performance, irrespective of whether it is applied ad-hoc or post-hoc.

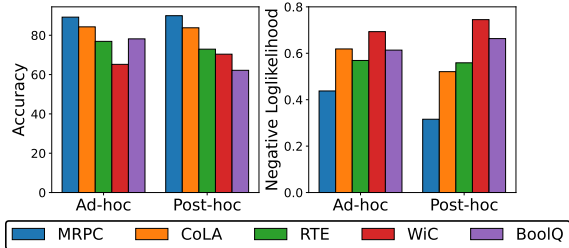


Figure 9: Effectiveness of **MonteCLoRA** in post-hoc operation.

7 Discussions

7.1 Use Cases

The previous section describes the sensitivity with existing low-rank adaptation-based fine-tuning methods. We also highlighted that given inappropriate hyperparameter selection, the existing techniques cannot demonstrate generalization capabilities post-fine-tuning process, defying the purpose of acquiring new knowledge during fine-tuning. In this section, we shed light on the training instability with these existing fine-tuning methods with two selected use cases.

Figure 10(a) illustrates a scenario where a LoRA fine-tuned RoBERTa-base model on the BoolQ task diverges. The training loss remains the same over the entire training period. Under the same hyperparameter configuration, **MonteCLoRA** achieves convergence with a steady drop in training loss. The training loss curve highlights that due to the posterior estimation, **MonteCLoRA** does not converge to any saddle point but rather robustly learns the global optima. A similar observation is made in Figure 10(b), where we observe abrasive optimization with LoRA fine-tuning strategy. RoBERTa-base with LoRA converges only af-

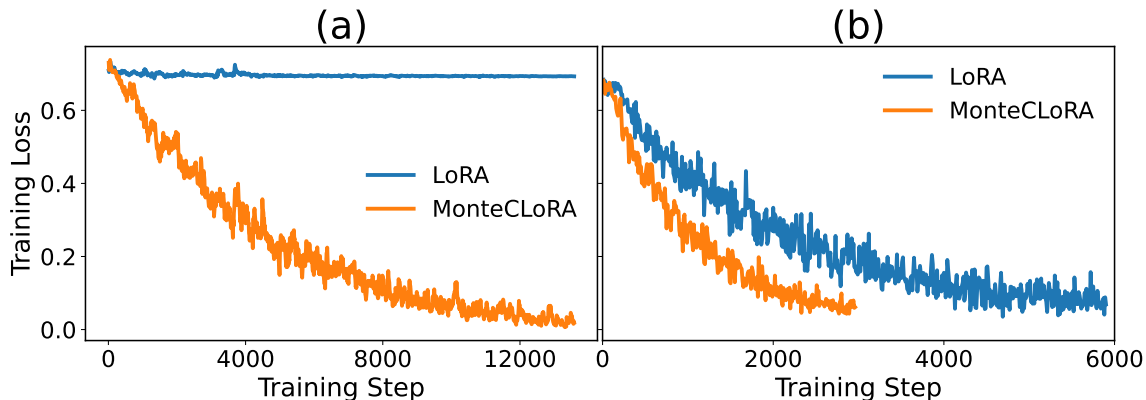


Figure 10: **(a)** Training loss curves on BoolQ with LoRA and MonteCLoRA fine-tuning. The loss curve with LoRA highlights its instability during fine-tuning, where the model eventually diverges. **(b)** Training loss curves on WiC, where MonteCLoRA achieves twice faster convergence than LoRA. For both the cases, we use RoBERTa-base with a learning rate of 3×10^{-4} and a batch size of 8 for both the fine-tuning strategies.

ter 6000 training steps. On the other hand, MonteCLoRA converges significantly faster in just < 3000 steps with a smoother optimization trajectory. With appropriate prior regularization, MonteCLoRA diminishes the sensitivity of the optimization process on hyperparameters like learning rates. Typically, with a high learning rate, a model can get struck at a local minima or even diverge, which is prominently seen with LoRA. However, this behavior is less frequent with MonteCLoRA.

7.2 Computational Complexity of MonteCLoRA

In Section 4, we highlighted the asymptotic complexity of MonteCLoRA, and showed that it introduces only $\mathcal{O}(1)$ additional parameters. In Table 10, we report the empirical time and memory complexities of MonteCLoRA and compare with LoRA and full fine-tuning. Due to sampling complexities, MonteCLoRA tends to have higher training time. We highlight the asymptotic time complexity of all the sampling processes involved in MonteCLoRA in Appendix A.4, where we observe that the runtime complexity of MonteCLoRA is typically $\mathcal{O}(r)$ times higher than that of LoRA. Therefore, when used with higher-rank matrices, the sampling usually requires longer time. When applied only to query, key, and value projection matrices of the RoBERTa-base model, LoRA fine-tuning takes a time similar to full fine-tuning. However, if LoRA is used on all the modules, the runtime increases by 68%. On the other hand, MonteCLoRA takes almost twice the time than LoRA when applied to query, key and value matrices. However, with more modules, the runtime only increases by 50% with MonteCLoRA. In terms of memory complexity, LoRA is more memory efficient than full fine-tuning, as it optimizes the gradient states of the training parameters. However, when applied to more modules, the GPU memory requirement increases for LoRA. Contrarily, MonteCLoRA does not scale similarly. The GPU memory requirement of MonteCLoRA is less than that of LoRA when applied to all of the RoBERTa-base model parameters. Another interesting observation is the computational invariance of the number of mixture

Method	Module	Num Samples	Runtime (in seconds)	GPU memory (in GB)
Full FT	-	-	859 \pm 35	31.4 \pm 0.6
LoRA	-	-	840 \pm 23	29.1 \pm 0.3
MonteCLoRA	QKV	4	1739 \pm 55	31.4 \pm 0.3
		8	1705 \pm 61	31.5 \pm 0.3
LoRA	-	-	1408 \pm 67	33.6 \pm 1.4
MonteCLoRA	All	4	2578 \pm 89	33.2 \pm 0.8
		8	2539 \pm 76	33.3 \pm 0.9

Table 10: Runtime and memory analysis of MonteCLoRA and LoRA with RoBERTa-base on the WiC task.

components in the Gaussian mixture model. Although we expect a higher runtime with more Gaussian components in the mixture, the runtime does not increase with the number of components. Due to hardware-level optimization, we can leverage a higher number of mixture components without costing any additional training time.

8 Conclusion

This paper introduced a Bayesian reparameterization of low-rank adaptation for efficiently fine-tuning LLMs. We highlighted the sensitivity of existing fine-tuning strategies and proposed MonteCLoRA that provides a robust and unbiased estimate of parameter-efficient fine-tuning. MonteCLoRA parameterizes low-rank fine-tuned parameters as a mixture of Gaussian with appropriate prior parameterization. With robust Monte Carlo estimates, MonteCLoRA reduces the sensitivity of the parameterized LLMs over the hyperparameters. Our thorough empirical study overmined the superiority of MonteCLoRA over the contemporary low-rank adaptation method in terms of performance and stability. Although the current work acknowledges the effectiveness of MonteCLoRA on low-rank parameterization regimes, the applicability of our method extends far beyond this. MonteCLoRA can be equally effective with the pre-trained LLM parameters. However, keeping the rising computation cost of fine-tuning LLMs, it is computationally more sensible to utilize MonteCLoRA with low-rank parameters rather than high-rank dense parameters. MonteCLoRA can also offer great flexibility where it can be used to ensure robustness even during pre-training of LLMs.

Acknowledgments and Disclosure of Funding

This work has been supported in part by J.P. Morgan AI Faculty Research Award. This paper was prepared for informational purposes in part by the Artificial Intelligence Research group of JPMorgan Chase & Co and its affiliates (“J.P. Morgan”) and is not a product of the Research Department of J.P. Morgan. J.P. Morgan makes no representation and warranty whatsoever and disclaims all liability, for the completeness, accuracy or reliability of the information contained herein. This document is not intended as investment research or investment advice, or a recommendation, offer or solicitation for the purchase or sale of any security, financial instrument, financial product or service, or to be used in any way for evaluating the merits of participating in any transaction, and shall not constitute a solici-

tation under any jurisdiction or to any person, if such solicitation under such jurisdiction or to such person would be unlawful.

References

- Aradhye Agarwal, Suhas K Ramesh, Ayan Sengupta, and Tanmoy Chakraborty. Step-by-step unmasking for parameter-efficient fine-tuning of large language models. *arXiv preprint arXiv:2408.14470*, 2024.
- Ebtesam Almazrouei, Hamza Alobeidli, Abdulaziz Alshamsi, Alessandro Cappelli, Ruxandra Cojocaru, M erouane Debbah,  tienne Goffinet, Daniel Hesslow, Julien Launay, Quentin Malartic, et al. The falcon series of open language models. *arXiv preprint arXiv:2311.16867*, 2023.
- Luisa Bentivogli, Peter Clark, Ido Dagan, and Danilo Giampiccolo. The fifth pascal recognizing textual entailment challenge. *TAC*, 7:8, 2009.
- Dan Biderman, Jose Gonzalez Ortiz, Jacob Portes, Mansheej Paul, Philip Greengard, Connor Jennings, Daniel King, Sam Havens, Vitaliy Chiley, Jonathan Frankle, et al. Lora learns less and forgets less. *arXiv preprint arXiv:2405.09673*, 2024.
- Yonatan Bisk, Rowan Zellers, Ronan Le Bras, Jianfeng Gao, and Yejin Choi. Piqa: Reasoning about physical commonsense in natural language, 2019. URL <https://arxiv.org/abs/1911.11641>.
- Yonatan Bisk, Rowan Zellers, Jianfeng Gao, Yejin Choi, et al. Piqa: Reasoning about physical commonsense in natural language. In *Proceedings of the AAAI conference on artificial intelligence*, volume 34, pages 7432–7439, 2020.
- Tom Brown, Benjamin Mann, Nick Ryder, Melanie Subbiah, Jared D Kaplan, Prafulla Dhariwal, Arvind Neelakantan, Pranav Shyam, Girish Sastry, Amanda Askell, et al. Language models are few-shot learners. *Advances in neural information processing systems*, 33:1877–1901, 2020.
- Hugh Chen, Scott Lundberg, and Su-In Lee. Checkpoint ensembles: Ensemble methods from a single training process. *arXiv preprint arXiv:1710.03282*, 2017.
- Christopher Clark, Kenton Lee, Ming-Wei Chang, Tom Kwiatkowski, Michael Collins, and Kristina Toutanova. Boolq: Exploring the surprising difficulty of natural yes/no questions. *arXiv preprint arXiv:1905.10044*, 2019.
- Peter Clark, Isaac Cowhey, Oren Etzioni, Tushar Khot, Ashish Sabharwal, Carissa Schoenick, and Oyvind Tafjord. Think you have solved question answering? try arc, the ai2 reasoning challenge. *arXiv preprint arXiv:1803.05457*, 2018.
- Ido Dagan, Oren Glickman, and Bernardo Magnini. The pascal recognising textual entailment challenge. In *Machine learning challenges workshop*, pages 177–190. Springer, 2005.

- Erik Daxberger, Agustinus Kristiadi, Alexander Immer, Runa Eschenhagen, Matthias Bauer, and Philipp Hennig. Laplace redux-effortless bayesian deep learning. *Advances in Neural Information Processing Systems*, 34:20089–20103, 2021.
- Zhijie Deng, Feng Zhou, and Jun Zhu. Accelerated linearized laplace approximation for bayesian deep learning. *Advances in Neural Information Processing Systems*, 35:2695–2708, 2022.
- Jacob Devlin, Ming-Wei Chang, Kenton Lee, and Kristina Toutanova. Bert: Pre-training of deep bidirectional transformers for language understanding. *arXiv preprint arXiv:1810.04805*, 2018.
- Ning Ding, Xingtai Lv, Qiaosen Wang, Yulin Chen, Bowen Zhou, Zhiyuan Liu, and Maosong Sun. Sparse low-rank adaptation of pre-trained language models. In *Proceedings of the 2023 Conference on Empirical Methods in Natural Language Processing*, pages 4133–4145, 2023.
- Bill Dolan and Chris Brockett. Automatically constructing a corpus of sentential paraphrases. In *Third International Workshop on Paraphrasing (IWP2005)*, 2005.
- Yarin Gal and Zoubin Ghahramani. Dropout as a bayesian approximation: Representing model uncertainty in deep learning. In *international conference on machine learning*, pages 1050–1059. PMLR, 2016.
- Guillaume Garrigos and Robert M. Gower. Handbook of convergence theorems for (stochastic) gradient methods, 2024. URL <https://arxiv.org/abs/2301.11235>.
- Saeed Ghadimi and Guanghui Lan. Stochastic first- and zeroth-order methods for nonconvex stochastic programming, 2013. URL <https://arxiv.org/abs/1309.5549>.
- Danilo Giampiccolo, Bernardo Magnini, Ido Dagan, and William B Dolan. The third pascal recognizing textual entailment challenge. In *Proceedings of the ACL-PASCAL workshop on textual entailment and paraphrasing*, pages 1–9, 2007.
- Chuan Guo, Geoff Pleiss, Yu Sun, and Kilian Q Weinberger. On calibration of modern neural networks. In *International conference on machine learning*, pages 1321–1330. PMLR, 2017.
- R Bar Haim, Ido Dagan, Bill Dolan, Lisa Ferro, Danilo Giampiccolo, Bernardo Magnini, and Idan Szpektor. The second pascal recognising textual entailment challenge. In *Proceedings of the Second PASCAL Challenges Workshop on Recognising Textual Entailment*, volume 7, pages 785–794, 2006.
- Neil Houlsby, Andrei Giurgiu, Stanislaw Jastrzebski, Bruna Morrone, Quentin De Larousilhe, Andrea Gesmundo, Mona Attariyan, and Sylvain Gelly. Parameter-efficient transfer learning for nlp. In *International conference on machine learning*, pages 2790–2799. PMLR, 2019.
- Jeremy Howard and Sebastian Ruder. Universal language model fine-tuning for text classification. *arXiv preprint arXiv:1801.06146*, 2018.

- Edward J Hu, yelong shen, Phillip Wallis, Zeyuan Allen-Zhu, Yuanzhi Li, Shean Wang, Lu Wang, and Weizhu Chen. LoRA: Low-rank adaptation of large language models. In *International Conference on Learning Representations*, 2022. URL <https://openreview.net/forum?id=nZeVKeeFYf9>.
- Zhiqiang Hu, Lei Wang, Yihuai Lan, Wanyu Xu, Ee-Peng Lim, Lidong Bing, Xing Xu, Soujanya Poria, and Roy Ka-Wei Lee. LLM-adapters: An adapter family for parameter-efficient fine-tuning of large language models. In *The 2023 Conference on Empirical Methods in Natural Language Processing*, 2023. URL <https://openreview.net/forum?id=gdUBK65fwn>.
- Pavel Izmailov, Dmitrii Podoprikin, Timur Garipov, Dmitry Vetrov, and Andrew Gordon Wilson. Averaging weights leads to wider optima and better generalization, 2019. URL <https://arxiv.org/abs/1803.05407>.
- Albert Q Jiang, Alexandre Sablayrolles, Arthur Mensch, Chris Bamford, Devendra Singh Chaplot, Diego de las Casas, Florian Bressand, Gianna Lengyel, Guillaume Lample, Lucile Saulnier, et al. Mistral 7b. *arXiv preprint arXiv:2310.06825*, 2023.
- Jared Kaplan, Sam McCandlish, Tom Henighan, Tom B Brown, Benjamin Chess, Rewon Child, Scott Gray, Alec Radford, Jeffrey Wu, and Dario Amodei. Scaling laws for neural language models. *arXiv preprint arXiv:2001.08361*, 2020.
- Diederik P Kingma. Auto-encoding variational bayes. *arXiv preprint arXiv:1312.6114*, 2013.
- Hector Levesque, Ernest Davis, and Leora Morgenstern. The winograd schema challenge. In *Thirteenth international conference on the principles of knowledge representation and reasoning*, 2012.
- Zonglin Li, Chong You, Srinadh Bhojanapalli, Daliang Li, Ankit Singh Rawat, Sashank J Reddi, Ke Ye, Felix Chern, Felix Yu, Ruiqi Guo, et al. The lazy neuron phenomenon: On emergence of activation sparsity in transformers. *arXiv preprint arXiv:2210.06313*, 2022.
- Haokun Liu, Derek Tam, Mohammed Muqeeth, Jay Mohta, Tenghao Huang, Mohit Bansal, and Colin A Raffel. Few-shot parameter-efficient fine-tuning is better and cheaper than in-context learning. *Advances in Neural Information Processing Systems*, 35:1950–1965, 2022a.
- Shih-Yang Liu, Chien-Yi Wang, Hongxu Yin, Pavlo Molchanov, Yu-Chiang Frank Wang, Kwang-Ting Cheng, and Min-Hung Chen. Dora: Weight-decomposed low-rank adaptation. *arXiv preprint arXiv:2402.09353*, 2024.
- Xiao Liu, Kaixuan Ji, Yicheng Fu, Weng Tam, Zhengxiao Du, Zhilin Yang, and Jie Tang. P-tuning: Prompt tuning can be comparable to fine-tuning across scales and tasks. In Smaranda Muresan, Preslav Nakov, and Aline Villavicencio, editors, *Proceedings of the 60th Annual Meeting of the Association for Computational Linguistics (Volume 2: Short Papers)*, pages 61–68, Dublin, Ireland, May 2022b. Association for Computational Linguistics. doi: 10.18653/v1/2022.acl-short.8. URL <https://aclanthology.org/2022.acl-short.8>.

- Yinhan Liu, Myle Ott, Naman Goyal, Jingfei Du, Mandar Joshi, Danqi Chen, Omer Levy, Mike Lewis, Luke Zettlemoyer, and Veselin Stoyanov. Roberta: A robustly optimized bert pretraining approach. *arXiv preprint arXiv:1907.11692*, 2019.
- Todor Mihaylov, Peter Clark, Tushar Khot, and Ashish Sabharwal. Can a suit of armor conduct electricity? a new dataset for open book question answering. *arXiv preprint arXiv:1809.02789*, 2018.
- Theodore Papamarkou, Maria Skoularidou, Konstantina Palla, Laurence Aitchison, Julyan Arbel, David Dunson, Maurizio Filippone, Vincent Fortuin, Philipp Hennig, José Miguel Hernández-Lobato, Aliaksandr Hubin, Alexander Immer, Theofanis Karaletsos, Mohammad Emtiyaz Khan, Agustinus Kristiadi, Yingzhen Li, Stephan Mandt, Christopher Nemeth, Michael A Osborne, Tim G. J. Rudner, David Rügamer, Yee Whye Teh, Max Welling, Andrew Gordon Wilson, and Ruqi Zhang. Position: Bayesian deep learning is needed in the age of large-scale AI. In Ruslan Salakhutdinov, Zico Kolter, Katherine Heller, Adrian Weller, Nuria Oliver, Jonathan Scarlett, and Felix Berkenkamp, editors, *Proceedings of the 41st International Conference on Machine Learning*, volume 235 of *Proceedings of Machine Learning Research*, pages 39556–39586. PMLR, 21–27 Jul 2024a. URL <https://proceedings.mlr.press/v235/papamarkou24b.html>.
- Theodore Papamarkou, Maria Skoularidou, Konstantina Palla, Laurence Aitchison, Julyan Arbel, David Dunson, Maurizio Filippone, Vincent Fortuin, Philipp Hennig, José Miguel Hernández-Lobato, Aliaksandr Hubin, Alexander Immer, Theofanis Karaletsos, Mohammad Emtiyaz Khan, Agustinus Kristiadi, Yingzhen Li, Stephan Mandt, Christopher Nemeth, Michael A. Osborne, Tim G. J. Rudner, David Rügamer, Yee Whye Teh, Max Welling, Andrew Gordon Wilson, and Ruqi Zhang. Position: Bayesian deep learning is needed in the age of large-scale ai, 2024b. URL <https://arxiv.org/abs/2402.00809>.
- Jonas Pfeiffer, Aishwarya Kamath, Andreas Rücklé, Kyunghyun Cho, and Iryna Gurevych. Adapterfusion: Non-destructive task composition for transfer learning. *arXiv preprint arXiv:2005.00247*, 2020.
- Mohammad Taher Pilehvar and Jose Camacho-Collados. Wic: the word-in-context dataset for evaluating context-sensitive meaning representations. *arXiv preprint arXiv:1808.09121*, 2018.
- Colin Raffel, Noam Shazeer, Adam Roberts, Katherine Lee, Sharan Narang, Michael Matena, Yanqi Zhou, Wei Li, and Peter J Liu. Exploring the limits of transfer learning with a unified text-to-text transformer. *Journal of machine learning research*, 21(140): 1–67, 2020.
- Keisuke Sakaguchi, Ronan Le Bras, Chandra Bhagavatula, and Yejin Choi. Winogrande: An adversarial winograd schema challenge at scale. *Communications of the ACM*, 64(9): 99–106, 2021.
- Maarten Sap, Hannah Rashkin, Derek Chen, Ronan LeBras, and Yejin Choi. Socialiqa: Commonsense reasoning about social interactions. *arXiv preprint arXiv:1904.09728*, 2019.

- Ayan Sengupta, Shantanu Dixit, Md Shad Akhtar, and Tanmoy Chakraborty. A good learner can teach better: Teacher-student collaborative knowledge distillation. In *The Twelfth International Conference on Learning Representations*, 2024. URL <https://openreview.net/forum?id=Ixi4j6LtdX>.
- Joram Soch, The Book of Statistical Proofs, Maja, Pietro Monticone, Thomas J. Faulkenberry, Alex Kipnis, Kenneth Petrykowski, Carsten Alfeld, Heiner Atze, Adam Knapp, Ciarán D. McInerney, Lo4ding00, and amvosk. *StatProofBook/StatProofBook.github.io: StatProofBook 2023*. Zenodo, January 2024. doi: 10.5281/zenodo.10495684. URL <https://doi.org/10.5281/zenodo.10495684>.
- Yi-Lin Sung, Varun Nair, and Colin A Raffel. Training neural networks with fixed sparse masks. *Advances in Neural Information Processing Systems*, 34:24193–24205, 2021.
- Hugo Touvron, Thibaut Lavril, Gautier Izacard, Xavier Martinet, Marie-Anne Lachaux, Timothée Lacroix, Baptiste Rozière, Naman Goyal, Eric Hambro, Faisal Azhar, et al. Llama: Open and efficient foundation language models. *arXiv preprint arXiv:2302.13971*, 2023.
- Christophe Tribes, Sacha Benarroch-Lelong, Peng Lu, and Ivan Kobyzev. Hyperparameter optimization for large language model instruction-tuning. *arXiv preprint arXiv:2312.00949*, 2023.
- Mojtaba Valipour, Mehdi Rezagholizadeh, Ivan Kobyzev, and Ali Ghodsi. Dylora: Parameter efficient tuning of pre-trained models using dynamic search-free low-rank adaptation. *arXiv preprint arXiv:2210.07558*, 2022.
- Ashish Vaswani, Noam Shazeer, Niki Parmar, Jakob Uszkoreit, Llion Jones, Aidan N Gomez, Lukasz Kaiser, and Illia Polosukhin. Attention is all you need. *Advances in neural information processing systems*, 30, 2017.
- Alex Wang, Amanpreet Singh, Julian Michael, Felix Hill, Omer Levy, and Samuel R Bowman. Glue: A multi-task benchmark and analysis platform for natural language understanding. *arXiv preprint arXiv:1804.07461*, 2018.
- Alex Wang, Yada Pruksachatkun, Nikita Nangia, Amanpreet Singh, Julian Michael, Felix Hill, Omer Levy, and Samuel Bowman. Superglue: A stickier benchmark for general-purpose language understanding systems. *Advances in neural information processing systems*, 32, 2019.
- Hao Wang and Dit-Yan Yeung. A survey on bayesian deep learning. *ACM computing surveys (csur)*, 53(5):1–37, 2020.
- Alex Warstadt, Amanpreet Singh, and Samuel R Bowman. Neural network acceptability judgments. *Transactions of the Association for Computational Linguistics*, 7:625–641, 2019.
- Andrew G Wilson and Pavel Izmailov. Bayesian deep learning and a probabilistic perspective of generalization. *Advances in neural information processing systems*, 33:4697–4708, 2020.

- Thomas Wolf, Lysandre Debut, Victor Sanh, Julien Chaumond, Clement Delangue, Anthony Moi, Pierric Cistac, Tim Rault, Rémi Louf, Morgan Funtowicz, Joe Davison, Sam Shleifer, Patrick von Platen, Clara Ma, Yacine Jernite, Julien Plu, Canwen Xu, Teven Le Scao, Sylvain Gugger, Mariama Drame, Quentin Lhoest, and Alexander M. Rush. Transformers: State-of-the-art natural language processing. In *Proceedings of the 2020 Conference on Empirical Methods in Natural Language Processing: System Demonstrations*, pages 38–45, Online, October 2020. Association for Computational Linguistics. URL <https://www.aclweb.org/anthology/2020.emnlp-demos.6>.
- Xingyu Xie, Kuangyu Ding, Shuicheng Yan, Kim-Chuan Toh, and Tianwen Wei. Optimization hyper-parameter laws for large language models. *arXiv preprint arXiv:2409.04777*, 2024.
- Adam X. Yang, Maxime Robeyns, Xi Wang, and Laurence Aitchison. Bayesian low-rank adaptation for large language models. In *The Twelfth International Conference on Learning Representations*, 2024. URL <https://openreview.net/forum?id=FJiUyz0F1m>.
- Elad Ben Zaken, Shauli Ravfogel, and Yoav Goldberg. Bitfit: Simple parameter-efficient fine-tuning for transformer-based masked language-models. *arXiv preprint arXiv:2106.10199*, 2021.
- Qingru Zhang, Minshuo Chen, Alexander Bukharin, Pengcheng He, Yu Cheng, Weizhu Chen, and Tuo Zhao. Adaptive budget allocation for parameter-efficient fine-tuning. In *The Eleventh International Conference on Learning Representations*, 2023.
- Shujian Zhang, Xinjie Fan, Bo Chen, and Mingyuan Zhou. Bayesian attention belief networks. In *International Conference on Machine Learning*, pages 12413–12426. PMLR, 2021.
- Wayne Xin Zhao, Kun Zhou, Junyi Li, Tianyi Tang, Xiaolei Wang, Yupeng Hou, Yingqian Min, Beichen Zhang, Junjie Zhang, Zican Dong, et al. A survey of large language models. *arXiv preprint arXiv:2303.18223*, 2023.

Appendix A.

A.1 Datasets

A.1.1 NATURAL LANGUAGE UNDERSTANDING

The General Language Understanding Evaluation (GLUE) (Wang et al., 2018) and SuperGLUE benchmarks (Wang et al., 2019) evaluate the language understanding capabilities of LLMs. All the datasets in GLUE and SuperGLUE are obtained from <https://gluebenchmark.com/> and <https://super.gluebenchmark.com/>, respectively. We elaborate on the GLUE and SuperGLUE tasks as follows:

CoLA (Warstadt et al., 2019), or The Corpus of Linguistic Acceptability, comprises acceptability judgments from books and journal articles. The task is to indicate the grammatical correctness of the given sentence as “acceptable” or “unacceptable” using the Matthews correlation coefficient as the evaluation metric.

MRPC (Dolan and Brockett, 2005), or Microsoft Research Paraphrase Corpus, comprises pairs of sentences extracted from online news sources. The objective is to predict whether the provided pair of sentences are paraphrases of each other or not.

RTE (Dagan et al., 2005; Haim et al., 2006; Giampiccolo et al., 2007; Bentivogli et al., 2009), or Recognizing Textual Entailment, are formed by combining a series of annual textual entailment challenges. The task comprises categorizing whether the two sentences entail each other.

BoolQ (Clark et al., 2019), or Boolean Questions, involves binary inquiries sourced from the Google search engine. These questions are combined with pertinent paragraphs extracted from Wikipedia articles, ensuring that the provided paragraphs contain accurate answers to the queries.

WiC (Pilehvar and Camacho-Collados, 2018), or Word-in-Context, is a word sense disambiguation task that involves binary classification of sentence pairs. Within this task, two text snippets are presented, each featuring a word with multiple potential meanings. The objective is to determine whether the specified word holds the same meaning in both sentences.

A.1.2 COMMONSENSE REASONING

PiQA (Bisk et al., 2019), or Physical Interaction: Question Answering, is a reasoning benchmark based on physical interactions in everyday situations. This benchmark comprises questions with two choices, out of which one option is correct based on realistic understanding of the world.

SiQA (Sap et al., 2019) or Social Interaction Question Answer, is a reasoning benchmark based on testing social commonsense intelligence. SiQA consists of multiple choice questions, with each question describing a social scenario, followed by a query with multiple options, one of which is the correct scenario representing the protagonist’s likely intention.

Winogrande (Sakaguchi et al., 2021) is a commonsense reasoning task inspired by the WSC (Levesque et al., 2012). The goal of the task is to choose the correct choice given two choices.

ARC-easy & **ARC-challenge** (Clark et al., 2018) comprise the AI2 Reasoning Challenge (ARC) partitioned into easy (ARC-e) and challenging set (ARC-c). The datasets consist of grade-school science questions in multiple choice format.

OpenBookQA (Mihaylov et al., 2018) contains elementary-level science questions in the form of multiple choices requiring additional commonsense knowledge.

A.2 Distributions and Reparameterization for Differentiable Backpropagation

Reparameterization trick (Kingma, 2013) is often used to make sampling from a probability distribution differentiable, where the distribution parameters are unknown and learnable parameters of the model. Our method is heavily dependent on reparameterized sampling from different distributions, their correctness and their differentiability. Here we describe the reparameterization techniques for the different probability distributions used in the paper.

A.2.1 MULTIVARIATE GAUSSIAN

The Normal distribution, also known as the Gaussian distribution, is one of the most widely used probability distributions in statistics and machine learning. It is fundamental in describing continuous data and plays a crucial role in various statistical methodologies, including hypothesis testing, confidence interval estimation, and regression analysis. The Normal distribution is parameterized by two key components

- **Mean ($\boldsymbol{\mu}$)**, a p -dimensional vector representing the central tendency or the expected value of the distribution. It determines the location of the peak of the distribution in the p -dimensional space.
- **Covariance Matrix ($\boldsymbol{\Sigma}$)**, a symmetric, positive-definite $p \times p$ matrix that encapsulates the variance of each dimension and the covariance between different dimensions. It defines the shape and orientation of the distribution.

We denote a normally distributed random vector as $\mathbf{x} \sim \mathcal{N}(\boldsymbol{\mu}, \boldsymbol{\Sigma})$. The probability density function of the Normal distribution is given by

$$f_{\mathbf{x}}(\mathbf{x}) = \frac{1}{(2\pi)^{p/2} |\boldsymbol{\Sigma}|^{1/2}} \exp\left(-\frac{1}{2}(\mathbf{x} - \boldsymbol{\mu})^\top \boldsymbol{\Sigma}^{-1}(\mathbf{x} - \boldsymbol{\mu})\right),$$

where,

- $(\mathbf{x} - \boldsymbol{\mu})$ is the deviation of the random vector from the mean.
- $\boldsymbol{\Sigma}^{-1}$ is the inverse of the covariance matrix.
- $|\boldsymbol{\Sigma}|$ denotes the determinant of $\boldsymbol{\Sigma}$.

Reparameterized Sampling and Proof of Differentiability

Let $\mathbf{x} \sim \mathcal{N}(\boldsymbol{\mu}, \boldsymbol{\Sigma})$ be a random vector sampled from a multivariate normal distribution, where $\boldsymbol{\mu} \in \mathbb{R}^d$ is the mean vector, and $\boldsymbol{\Sigma} \in \mathbb{R}^{d \times d}$ is the covariance matrix. In the reparameterization trick, we express the sample \mathbf{x} as,

$$\mathbf{x} = \boldsymbol{\mu} + \mathbf{L}\boldsymbol{\epsilon},$$

where $\boldsymbol{\epsilon} \sim \mathcal{N}(\mathbf{0}, \mathbf{I})$ is a standard normal vector, and \mathbf{L} is the Cholesky decomposition of the covariance matrix $\boldsymbol{\Sigma}$, such that $\boldsymbol{\Sigma} = \mathbf{L}\mathbf{L}^T$. We will prove that the reparameterized transformation $\mathbf{x} = \boldsymbol{\mu} + \mathbf{L}\boldsymbol{\epsilon}$ is differentiable with respect to both $\boldsymbol{\mu}$ and $\boldsymbol{\Sigma}$. The mean vector $\boldsymbol{\mu}$ appears linearly in the transformation

$$\mathbf{x} = \boldsymbol{\mu} + \mathbf{L}\boldsymbol{\epsilon}.$$

Since the transformation is linear with respect to $\boldsymbol{\mu}$, the derivative of \mathbf{x} with respect to $\boldsymbol{\mu}$ is,

$$\frac{\partial \mathbf{x}}{\partial \boldsymbol{\mu}} = \mathbf{I},$$

where \mathbf{I} is the identity matrix. Hence, \mathbf{x} is differentiable with respect to $\boldsymbol{\mu}$.

The covariance matrix $\boldsymbol{\Sigma}$ enters the transformation through Cholesky decomposition $\boldsymbol{\Sigma} = \mathbf{L}\mathbf{L}^T$. The Cholesky decomposition is a differentiable function of $\boldsymbol{\Sigma}$ as long as $\boldsymbol{\Sigma}$ is positive definite. Thus, the entries of the matrix \mathbf{L} are differentiable functions of the entries of $\boldsymbol{\Sigma}$. Since the transformation $\mathbf{x} = \boldsymbol{\mu} + \mathbf{L}\boldsymbol{\epsilon}$ depends linearly on \mathbf{L} , we can apply the chain rule to differentiate \mathbf{x} with respect to $\boldsymbol{\Sigma}$. Let $\mathbf{x} = f(\boldsymbol{\Sigma}, \boldsymbol{\epsilon}) = \boldsymbol{\mu} + g(\boldsymbol{\Sigma})\boldsymbol{\epsilon}$, where $g(\boldsymbol{\Sigma})$ is the Cholesky factor \mathbf{L} . The derivative of \mathbf{x} with respect to $\boldsymbol{\Sigma}$ is

$$\frac{\partial \mathbf{x}}{\partial \boldsymbol{\Sigma}} = \frac{\partial \mathbf{x}}{\partial \mathbf{L}} \cdot \frac{\partial \mathbf{L}}{\partial \boldsymbol{\Sigma}}.$$

Since \mathbf{x} is a linear transformation of \mathbf{L} , and \mathbf{L} is differentiable with respect to $\boldsymbol{\Sigma}$, \mathbf{x} is differentiable with respect to $\boldsymbol{\Sigma}$.

A.2.2 WISHART DISTRIBUTION

The Wishart distribution is a fundamental probability distribution in multivariate statistics, particularly in the context of covariance matrices. It serves as the conjugate prior for the covariance matrix of a multivariate normal distribution in Bayesian statistics and plays a crucial role in various statistical methodologies, including multivariate hypothesis testing and estimation. The Wishart distribution is parameterized by two key components:

- **Degrees of Freedom (ν)**, a positive integer representing the number of independent samples contributing to the covariance estimation. It must satisfy $\nu \geq p$, where p is the dimensionality of the covariance matrix.
- **Scale Matrix (\mathbf{V})**, a symmetric, positive-definite $p \times p$ matrix that serves as the scale or covariance matrix in the distribution. It encapsulates the variance and covariance structure of the underlying multivariate normal distribution.

We denote a Wishart-distributed random matrix as $\mathbf{W} \sim \mathcal{W}_p(\mathbf{V}, \nu)$. The probability density function of the Wishart distribution is given by,

$$f_{\mathbf{W}}(\mathbf{W}) = \frac{|\mathbf{W}|^{(\nu-p-1)/2} \exp\left(-\frac{1}{2}\text{tr}(\mathbf{V}^{-1}\mathbf{W})\right)}{2^{\nu p/2} |\mathbf{V}|^{\nu/2} \Gamma_p\left(\frac{\nu}{2}\right)}.$$

Reparameterized Sampling and Proof of Differentiability

Wishart distribution is the conjugate prior of the precision matrix (inverse covariance-matrix) of a multivariate Gaussian distribution with unknown variance. For sampling $\boldsymbol{\Sigma} \sim$

$\mathcal{W}_m(\mathbf{V}, n)$ with $\mathbf{V} \in \mathbb{R}^{m \times m}$ being the scale matrix and n degrees of freedom, we first calculate Cholesky decomposition $\mathbf{L}\mathbf{L}^T = \mathbf{V}$, with a lower triangular matrix \mathbf{L} . As \mathbf{V} is diagonal, \mathbf{L} can be directly calculated as

$$\begin{bmatrix} \sqrt{V_1} & & & \\ & \ddots & & \\ & & \ddots & \\ & & & \sqrt{V_m} \end{bmatrix}.$$

Next, we sample $\tilde{\Sigma} \sim \mathcal{W}_m(\mathbf{I}, n)$. The reparametrized variance matrix is $\Sigma = \mathbf{L}\tilde{\Sigma}\mathbf{L}^T$. Let $\Sigma \sim \mathcal{W}_p(\mathbf{V}, n)$ be a sample from the Wishart distribution, where $\mathbf{V} \in \mathbb{R}^{p \times p}$ is a positive-definite scale matrix, and n is the degrees of freedom.

The Cholesky decomposition relates \mathbf{V} and \mathbf{L} through the equation $\mathbf{V} = \mathbf{L}\mathbf{L}^T$. The elements of \mathbf{V} are quadratic functions of the elements of \mathbf{L} ,

$$V_{ij} = \sum_{k=1}^{\min(i,j)} \ell_{ik}\ell_{jk}.$$

This relationship is differentiable, and the partial derivatives of ℓ_{ij} with respect to V_{kl} are well-defined. Thus, \mathbf{L} is a differentiable function of \mathbf{V} . The reparameterized Wishart sample is given by,

$$\Sigma = \mathbf{L}\tilde{\Sigma}\mathbf{L}^T.$$

Using the chain rule, we compute the derivative of Σ with respect to \mathbf{V} as,

$$\frac{\partial \Sigma}{\partial \mathbf{V}} = \frac{\partial \Sigma}{\partial \mathbf{L}} \cdot \frac{\partial \mathbf{L}}{\partial \mathbf{V}}.$$

The differentiation of Σ with respect to \mathbf{V} proceeds as follows. Using the chain rule, we first differentiate Σ with respect to \mathbf{L} , and then differentiate \mathbf{L} with respect to \mathbf{V}

$$\frac{\partial \Sigma}{\partial \mathbf{V}} = \frac{\partial \Sigma}{\partial \mathbf{L}} \cdot \frac{\partial \mathbf{L}}{\partial \mathbf{V}}.$$

Since $\Sigma = \mathbf{L}\tilde{\Sigma}\mathbf{L}^T$, the derivative with respect to \mathbf{L} is,

$$\frac{\partial \Sigma}{\partial \mathbf{L}} = \frac{\partial}{\partial \mathbf{L}} \left(\mathbf{L}\tilde{\Sigma}\mathbf{L}^T \right) = \tilde{\Sigma}\mathbf{L}^T + \mathbf{L}\tilde{\Sigma}.$$

From the above, we can conclude that the reparamterised fromulation of Wishart Distribution retains its differentiability with respect to its parameters

A.2.3 DIRICHLET DISTRIBUTION

The Dirichlet distribution is a fundamental probability distribution in multivariate statistics, particularly in the context of modeling probabilities and proportions. It serves as the conjugate prior for the parameters of the multinomial distribution in Bayesian statistics and is widely used in various applications such as topic modeling, Bayesian mixture models, and compositional data analysis. The Dirichlet distribution is parameterized by two key components:

- **Number of Components (\mathbf{K})**, the number of components in the random vector or the dimension of the random vector is decided by this parameter.
- **Concentration Parameters ($\boldsymbol{\alpha}$)**, a vector of positive real numbers $\boldsymbol{\alpha} = (\alpha_1, \alpha_2, \dots, \alpha_K)$, where each $\alpha_i > 0$. These parameters control the shape of the distribution, influencing the variability and the mean of each component in the simplex.

We denote a Dirichlet-distributed random vector as $\boldsymbol{\theta} \sim \text{Dir}(\boldsymbol{\alpha})$, where $\boldsymbol{\theta} = (\theta_1, \theta_2, \dots, \theta_K)$ and $\sum_{i=1}^K \theta_i = 1$. The probability density function of the Dirichlet distribution is given by,

$$f_{\boldsymbol{\theta}}(\boldsymbol{\theta}) = \frac{1}{B(\boldsymbol{\alpha})} \prod_{i=1}^K \theta_i^{\alpha_i-1},$$

where

- $\theta_i \geq 0$ for all $i = 1, \dots, K$, and $\sum_{i=1}^K \theta_i = 1$.
- $B(\boldsymbol{\alpha})$ is the multivariate beta function, defined as

$$B(\boldsymbol{\alpha}) = \frac{\prod_{i=1}^K \Gamma(\alpha_i)}{\Gamma\left(\sum_{i=1}^K \alpha_i\right)}$$

- $\Gamma(\cdot)$ is the Gamma function.

Reparameterized Sampling and Proof of Differentiability

Suppose we want to sample $\boldsymbol{\pi} \sim \text{Dir}(\boldsymbol{\alpha})$, where $\boldsymbol{\alpha} = (\alpha_1, \dots, \alpha_K)$ is the concentration parameter. We first sample K independent Gamma-distributed variables $y_i \sim \text{Gamma}(\alpha_i, 1)$, for $i = 1, \dots, K$. To ensure differentiability of the sampling process, we apply the reparameterization trick by expressing each y_i as,

$$y_i = \alpha_i \cdot (-\log \epsilon_i),$$

where $\epsilon_i \sim \text{Uniform}(0, 1)$ is an independent uniform random variable. Finally, the reparameterized Dirichlet sample \boldsymbol{p} is obtained as follows.

We sample K independent Gamma-distributed variables $y_i \sim \text{Gamma}(\alpha_i, 1)$, for $i = 1, \dots, K$. The reparameterization of the Gamma distribution is given by,

$$y_i = g(\alpha_i, \epsilon_i) = \alpha_i \cdot (-\log(\epsilon_i)),$$

where $\epsilon_i \sim \text{Uniform}(0, 1)$. Since the transformation $g(\alpha_i, \epsilon_i)$ is differentiable with respect to α_i , we have,

$$\frac{\partial y_i}{\partial \alpha_i} = -\log(\epsilon_i).$$

Thus, y_i is differentiable with respect to α_i . After sampling y_i , we normalize the variables to obtain the Dirichlet sample,

$$p_i = \frac{y_i}{\sum_{j=1}^K y_j}.$$

The normalization is a smooth function of the y_i s, so the resulting p_i is differentiable as long as $\sum_{j=1}^K y_j > 0$ (which holds because each $y_i > 0$). The derivative of p_i with respect to y_i is,

$$\frac{\partial p_i}{\partial y_i} = \frac{\sum_{j=1}^K y_j - y_i}{\left(\sum_{j=1}^K y_j\right)^2}.$$

Since y_i is differentiable with respect to α_i , the sample $\mathbf{p} = \{p_1, p_2, \dots, p_K\}$ is differentiable with respect to $\boldsymbol{\alpha}$.

A.3 Calculation of KL Divergence Losses

For calculating the KL Divergence of the distributions used in this paper, we refer to Soch et al. (2024).

A.3.1 MULTIVARIATE NORMAL

Lemma 10 *Let \mathbf{x} be an $n \times 1$ random vector. Assume two multivariate normal distributions, P and Q specifying the probability distribution of \mathbf{x} as,*

$$P : \mathbf{x} \sim N(\mu_1, \Sigma_1)$$

$$Q : \mathbf{x} \sim N(\mu_2, \Sigma_2).$$

Then, the KL divergence of P from Q is given by,

$$KL[P||Q] = \frac{1}{2} \left[(\mu_2 - \mu_1)^T \Sigma_2^{-1} (\mu_2 - \mu_1) + \text{tr}(\Sigma_2^{-1} \Sigma_1) - \ln \frac{|\Sigma_1|}{|\Sigma_2|} - n \right].$$

Proof The KL divergence for a continuous random variable is given by,

$$KL[P||Q] = \int_X p(\mathbf{x}) \ln \frac{p(\mathbf{x})}{q(\mathbf{x})} d\mathbf{x}.$$

Applying this to the multivariate Gaussian distributions yields,

$$KL[P||Q] = \int_{\mathbb{R}^n} N(\mathbf{x}; \mu_1, \Sigma_1) \ln \frac{N(\mathbf{x}; \mu_1, \Sigma_1)}{N(\mathbf{x}; \mu_2, \Sigma_2)} d\mathbf{x} = \left\langle \ln \frac{N(\mathbf{x}; \mu_1, \Sigma_1)}{N(\mathbf{x}; \mu_2, \Sigma_2)} \right\rangle_{p(\mathbf{x})}.$$

Using the probability density function of the multivariate normal distribution, this becomes,

$$KL[P||Q] = \left\langle \frac{1}{2} \ln \frac{|\Sigma_2|}{|\Sigma_1|} - \frac{1}{2} (\mathbf{x} - \mu_1)^T \Sigma_1^{-1} (\mathbf{x} - \mu_1) + \frac{1}{2} (\mathbf{x} - \mu_2)^T \Sigma_2^{-1} (\mathbf{x} - \mu_2) \right\rangle_{p(\mathbf{x})}.$$

Now, using the fact that trace and expectation are both linear operators, we obtain,

$$KL[P||Q] = \frac{1}{2} \left(\ln \frac{|\Sigma_2|}{|\Sigma_1|} - \text{tr} [\Sigma_1^{-1} \langle (\mathbf{x} - \mu_1)(\mathbf{x} - \mu_1)^T \rangle_{p(\mathbf{x})}] + \text{tr} [\Sigma_2^{-1} (\langle \mathbf{x}\mathbf{x}^T \rangle_{p(\mathbf{x})} - 2\mu_2 \langle \mathbf{x}^T \rangle_{p(\mathbf{x})} + \mu_2 \mu_2^T)] \right).$$

Using the expectation formulas for linear and quadratic forms for the multivariate normal distribution

$$\langle A\mathbf{x} \rangle = A\mu, \quad \langle \mathbf{x}^T A\mathbf{x} \rangle = \mu^T A\mu + \text{tr}(A\Sigma).$$

We substitute these into the KL divergence expression to get,

$$KL[P||Q] = \frac{1}{2} \left(\ln \frac{|\Sigma_2|}{|\Sigma_1|} - n + \text{tr}(\Sigma_2^{-1}\Sigma_1) + (\mu_2 - \mu_1)^T \Sigma_2^{-1} (\mu_2 - \mu_1) \right).$$

Finally, rearranging the terms gives,

$$KL[P||Q] = \frac{1}{2} \left[(\mu_2 - \mu_1)^T \Sigma_2^{-1} (\mu_2 - \mu_1) + \text{tr}(\Sigma_2^{-1}\Sigma_1) - \ln \frac{|\Sigma_1|}{|\Sigma_2|} - n \right].$$

For **MonteCLoRA**, the P and Q distributions are $\mathcal{N}(\boldsymbol{\mu}, \boldsymbol{\Sigma}_1)$ and $\mathcal{N}(\boldsymbol{\mu}, \mathbf{I})$, respectively. The KL Divergence between them is calculated as,

$$KL[P||Q] = \frac{1}{2} \left[(\boldsymbol{\mu} - \boldsymbol{\mu})^T \mathbf{I}^{-1} (\boldsymbol{\mu} - \boldsymbol{\mu}) + \text{tr}(\mathbf{I}^{-1}\boldsymbol{\Sigma}_1) - \ln \frac{|\boldsymbol{\Sigma}_1|}{|\mathbf{I}|} - n \right].$$

On further simplification, we get,

$$KL[P||Q] = \frac{1}{2} [\text{tr}(\boldsymbol{\Sigma}_1) - \ln |\boldsymbol{\Sigma}_1| - n].$$

■

A.3.2 WISHART DISTRIBUTION

Lemma 11 *Let S be a $p \times p$ random matrix. Assume two Wishart distributions, P and Q specifying the probability distribution of S as,*

$$P : S \sim W(V_1, n_1), \quad Q : S \sim W(V_2, n_2).$$

Then, the KL divergence of P from Q is given by,

$$KL[P||Q] = \frac{1}{2} \left[n_2 (\ln |V_2| - \ln |V_1|) + n_1 \text{tr}(V_2^{-1}V_1) + 2 \ln \frac{\Gamma_p\left(\frac{n_2}{2}\right)}{\Gamma_p\left(\frac{n_1}{2}\right)} + (n_1 - n_2) \psi_p\left(\frac{n_1}{2}\right) - n_1 p \right].$$

where $\Gamma_p(x)$ is the multivariate gamma function

$$\Gamma_p(x) = \pi^{\frac{p(p-1)}{4}} \prod_{j=1}^p \Gamma\left(x - \frac{j-1}{2}\right),$$

and $\psi_p(x)$ is the multivariate digamma function

$$\psi_p(x) = \frac{d \ln \Gamma_p(x)}{dx} = \sum_{j=1}^p \psi\left(x - \frac{j-1}{2}\right).$$

Proof The KL divergence for a continuous random variable is given by,

$$KL[P||Q] = \int_X p(x) \ln \frac{p(x)}{q(x)} dx.$$

Applied to the Wishart distributions, we get,

$$KL[P||Q] = \int_S p_W(S; V_1, n_1) \ln \frac{p_W(S; V_1, n_1)}{p_W(S; V_2, n_2)} dS.$$

Using the probability density function of the Wishart distribution, this becomes,

$$\begin{aligned} KL[P||Q] &= \left\langle \ln \frac{\frac{1}{\sqrt{2^{n_1 p} |V_1|^{n_1} \Gamma_p(\frac{n_1}{2})}} \cdot |S|^{(n_1 - p - 1)/2} \cdot \exp \left[-\frac{1}{2} \text{tr} (V_1^{-1} S) \right]}{\frac{1}{\sqrt{2^{n_2 p} |V_2|^{n_2} \Gamma_p(\frac{n_2}{2})}} \cdot |S|^{(n_2 - p - 1)/2} \cdot \exp \left[-\frac{1}{2} \text{tr} (V_2^{-1} S) \right]} \right\rangle_{p(S)} \\ &= \left\langle \ln \left(\sqrt{2^{(n_2 - n_1)p}} \cdot \frac{|V_2|^{n_2}}{|V_1|^{n_1}} \cdot \frac{\Gamma_p(\frac{n_2}{2})}{\Gamma_p(\frac{n_1}{2})} \cdot |S|^{(n_1 - n_2)/2} \cdot \exp \left[-\frac{1}{2} \text{tr} (V_1^{-1} S) + \frac{1}{2} \text{tr} (V_2^{-1} S) \right] \right) \right\rangle_{p(S)} \\ &= \left\langle \frac{(n_2 - n_1)p}{2} \ln 2 + \frac{n_2}{2} \ln |V_2| - \frac{n_1}{2} \ln |V_1| + \ln \frac{\Gamma_p(\frac{n_2}{2})}{\Gamma_p(\frac{n_1}{2})} \right. \\ &\quad \left. + \frac{n_1 - n_2}{2} \ln |S| - \frac{1}{2} \text{tr} (V_1^{-1} S) + \frac{1}{2} \text{tr} (V_2^{-1} S) \right\rangle_{p(S)} \\ &= \frac{(n_2 - n_1)p}{2} \ln 2 + \frac{n_2}{2} \ln |V_2| - \frac{n_1}{2} \ln |V_1| + \ln \frac{\Gamma_p(\frac{n_2}{2})}{\Gamma_p(\frac{n_1}{2})} \\ &\quad + \frac{n_1 - n_2}{2} \langle \ln |S| \rangle_{p(S)} - \frac{1}{2} \langle \text{tr} (V_1^{-1} S) \rangle_{p(S)} + \frac{1}{2} \langle \text{tr} (V_2^{-1} S) \rangle_{p(S)}. \end{aligned}$$

Using the expected value of a Wishart random matrix $S \sim W(V, n)$, we get

$$\langle S \rangle = nV.$$

Therefore, the expected value of the trace becomes

$$\langle \text{tr}(AS) \rangle = \text{tr}(A \langle S \rangle) = n \text{tr}(AV),$$

and the expected value of a Wishart log-determinant is

$$\langle \ln |S| \rangle = \psi_p \left(\frac{n}{2} \right) + p \ln 2 + \ln |V|.$$

Substituting these expectations, we get,

$$\begin{aligned} KL[P, ||, Q] &= \frac{(n_2 - n_1)p}{2} \ln 2 + \frac{n_2}{2} \ln |V_2| - \frac{n_1}{2} \ln |V_1| + \ln \frac{\Gamma_p(\frac{n_2}{2})}{\Gamma_p(\frac{n_1}{2})} \\ &\quad + \frac{n_1 - n_2}{2} \left[\psi_p \left(\frac{n_1}{2} \right) + p \cdot \ln 2 + \ln |V_1| \right] - \frac{n_1}{2} \text{tr} (V_1^{-1} V_1) + \frac{n_1}{2} \text{tr} (V_2^{-1} V_1) \\ &= \frac{n_2}{2} (\ln |V_2| - \ln |V_1|) + \ln \frac{\Gamma_p(\frac{n_2}{2})}{\Gamma_p(\frac{n_1}{2})} + \frac{n_1 - n_2}{2} \psi_p \left(\frac{n_1}{2} \right) - \frac{n_1}{2} \text{tr} (I_p) + \frac{n_1}{2} \text{tr} (V_2^{-1} V_1) \\ &= \frac{1}{2} \left[n_2 (\ln |V_2| - \ln |V_1|) + n_1 \text{tr} (V_2^{-1} V_1) + 2 \ln \frac{\Gamma_p(\frac{n_2}{2})}{\Gamma_p(\frac{n_1}{2})} + (n_1 - n_2) \psi_p \left(\frac{n_1}{2} \right) - n_1 p \right]. \end{aligned}$$

$$KL[P||Q] = \frac{1}{2} \left[n_2 (\ln |V_2| - \ln |V_1|) + n_1 \text{tr}(V_2^{-1}V_1) + 2 \ln \frac{\Gamma_p\left(\frac{n_2}{2}\right)}{\Gamma_p\left(\frac{n_1}{2}\right)} + (n_1 - n_2)\psi_p\left(\frac{n_1}{2}\right) - n_1 p \right].$$

For MonteCLoRA, we have taken $n_2 = n_1$ and V_2 is identity. On ignoring constants, the final KL divergence loss for our method is calculated as,

$$KL[P||Q] = \frac{1}{2} [-n_1 \ln |V_1| + n_1 \text{tr}(V_1)].$$

■

A.3.3 DIRICHLET DISTRIBUTION

Lemma 12 *Let \mathbf{x} be a $k \times 1$ random vector. Assume two Dirichlet distributions, P and Q , specifying the probability distribution of \mathbf{x} as,*

$$P : \mathbf{x} \sim \text{Dir}(\alpha_1), \quad Q : \mathbf{x} \sim \text{Dir}(\alpha_2).$$

Then, the KL divergence of P from Q is given by,

$$KL[P||Q] = \ln \frac{\Gamma\left(\sum_{i=1}^k \alpha_{1,i}\right)}{\Gamma\left(\sum_{i=1}^k \alpha_{2,i}\right)} + \sum_{i=1}^k \ln \frac{\Gamma(\alpha_{2,i})}{\Gamma(\alpha_{1,i})} + \sum_{i=1}^k (\alpha_{1,i} - \alpha_{2,i}) \left[\psi(\alpha_{1,i}) - \psi\left(\sum_{i=1}^k \alpha_{1,i}\right) \right].$$

Proof The KL divergence for a continuous random variable is given by,

$$KL[P||Q] = \int_X p(\mathbf{x}) \ln \frac{p(\mathbf{x})}{q(\mathbf{x})} d\mathbf{x}.$$

Applied to the Dirichlet distributions, we get,

$$KL[P||Q] = \int_{X_k} \text{Dir}(\mathbf{x}; \alpha_1) \ln \frac{\text{Dir}(\mathbf{x}; \alpha_1)}{\text{Dir}(\mathbf{x}; \alpha_2)} d\mathbf{x} = \left\langle \ln \frac{\text{Dir}(\mathbf{x}; \alpha_1)}{\text{Dir}(\mathbf{x}; \alpha_2)} \right\rangle_{p(\mathbf{x})}.$$

Here, X_k is the set $\{\mathbf{x} \in \mathbb{R}^k \mid \sum_{i=1}^k x_i = 1, 0 \leq x_i \leq 1, i = 1, \dots, k\}$. Using the probability density function of the Dirichlet distribution, this becomes,

$$KL[P||Q] = \left\langle \ln \frac{\frac{\Gamma(\sum_{i=1}^k \alpha_{1,i})}{\prod_{i=1}^k \Gamma(\alpha_{1,i})} \prod_{i=1}^k x_i^{\alpha_{1,i}-1}}{\frac{\Gamma(\sum_{i=1}^k \alpha_{2,i})}{\prod_{i=1}^k \Gamma(\alpha_{2,i})} \prod_{i=1}^k x_i^{\alpha_{2,i}-1}} \right\rangle_{p(\mathbf{x})}.$$

Simplifying this expression, we get,

$$KL[P||Q] = \left\langle \ln \left(\frac{\Gamma\left(\sum_{i=1}^k \alpha_{1,i}\right) \prod_{i=1}^k \Gamma(\alpha_{2,i})}{\Gamma\left(\sum_{i=1}^k \alpha_{2,i}\right) \prod_{i=1}^k \Gamma(\alpha_{1,i})} \prod_{i=1}^k x_i^{\alpha_{1,i}-\alpha_{2,i}} \right) \right\rangle_{p(\mathbf{x})}.$$

$$KL[P||Q] = \ln \frac{\Gamma\left(\sum_{i=1}^k \alpha_{1,i}\right)}{\Gamma\left(\sum_{i=1}^k \alpha_{2,i}\right)} + \sum_{i=1}^k \ln \frac{\Gamma(\alpha_{2,i})}{\Gamma(\alpha_{1,i})} + \sum_{i=1}^k (\alpha_{1,i} - \alpha_{2,i}) \langle \ln x_i \rangle_{p(\mathbf{x})}.$$

Using the expected value of the logarithm of a Dirichlet random variable $\mathbf{x} \sim \text{Dir}(\alpha)$

$$\langle \ln x_i \rangle = \psi(\alpha_i) - \psi\left(\sum_{i=1}^k \alpha_i\right),$$

the KL divergence becomes,

$$KL[P||Q] = \ln \frac{\Gamma\left(\sum_{i=1}^k \alpha_{1,i}\right)}{\Gamma\left(\sum_{i=1}^k \alpha_{2,i}\right)} + \sum_{i=1}^k \ln \frac{\Gamma(\alpha_{2,i})}{\Gamma(\alpha_{1,i})} + \sum_{i=1}^k (\alpha_{1,i} - \alpha_{2,i}) \left[\psi(\alpha_{1,i}) - \psi\left(\sum_{i=1}^k \alpha_{1,i}\right) \right].$$

■

A.4 Complexity Analysis of Sampling

Training MonteCLoRA involves sampling from three different distributions. Therefore, it is essential to analyze the complexity of sampling from these distributions.

A.4.1 SAMPLING FROM THE WISHART DISTRIBUTION

1. **Cholesky Decomposition of the Scale Matrix.** The time complexity of computing the Cholesky decomposition for a $p \times p$ matrix is typically $\mathcal{O}(p^3)$. However, since we are using a diagonal prior, the time complexity reduces to $\mathcal{O}(p)$ or $\mathcal{O}(r)$, as we are only sampling for LoRA A , and the prior is $r \times r$.
2. **Sampling from the Standard Wishart Distribution $\tilde{\Sigma} \sim \mathcal{W}_p(\mathbf{I}, k)$.** We generate k independent samples from a multivariate normal distribution $\mathcal{N}(\mathbf{0}, \mathbf{I}_p)$, with each sample involving p values. Generating the covariance matrix for each sample takes $\mathcal{O}(p^2)$ time. Therefore, the total time complexity for generating k samples is $\mathcal{O}(kp^2)$. In our context, this corresponds to $\mathcal{O}(n_{\text{in}}r^2)$.
3. **Reparameterization $\Sigma = \mathbf{L}\tilde{\Sigma}\mathbf{L}^T$.** The reparameterization step involves matrix multiplication and thus has a time complexity of $\mathcal{O}(p^3)$. In our case, it is $\mathcal{O}(r^3)$.

The total time complexity is $\mathcal{O}(r^3 + n_{\text{in}}r^2)$. Since $r \ll \min(n_{\text{in}}, n_{\text{out}})$, the complexity is heavily influenced by n_{in} . To mitigate this problem, we reduce the degrees of freedom to $\mathcal{O}(r)$. In practice, we found little difference between two degrees of freedom; therefore, we use the Wishart prior with degrees of freedom r .

A.4.2 SAMPLING FROM THE DIRICHLET DISTRIBUTION

The time complexity of sampling from the Dirichlet distribution using the reparameterization trick can be broken down into the following steps

1. **Reparameterization via Gamma Distribution.** Sampling from a Gamma distribution with shape parameter α_i and scale parameter 1 has time complexity $\mathcal{O}(1)$ for each variable y_i . Sampling N independent Gamma-distributed variables takes $\mathcal{O}(N)$ time.
2. **Normalization Step.** After generating Gamma-distributed variables y_i , we normalize them to produce the Dirichlet-distributed sample $\mathbf{p} = (p_1, \dots, p_N)$. Calculating the denominator involves a summation taking $\mathcal{O}(N)$ time, and normalizing each variable takes $\mathcal{O}(1)$ time. Therefore, the total time complexity for the normalization step is $\mathcal{O}(N)$.

Thus, the total time complexity of sampling from a Dirichlet distribution is $\mathcal{O}(N)$.

A.4.3 SAMPLING FROM A MULTIVARIATE NORMAL DISTRIBUTION

The time complexity of sampling from a multivariate normal distribution using the reparameterization trick is as follows

1. **Cholesky Decomposition of the Covariance Matrix.** The time complexity for computing the Cholesky decomposition of a $d \times d$ covariance matrix Σ is $\mathcal{O}(d^3)$. Since we use a diagonal covariance matrix, the complexity reduces to $\mathcal{O}(d)$. For us, it is $\mathcal{O}(r)$.
2. **Sampling from the Standard Normal Distribution.** The time complexity for generating a vector of d standard normal variables is $\mathcal{O}(d)$. For our case, this is $\mathcal{O}(r)$.
3. **Reparameterization $\mathbf{x} = \boldsymbol{\mu} + \mathbf{L}\boldsymbol{\epsilon}$.** The matrix-vector multiplication $\mathbf{L}\boldsymbol{\epsilon}$ involves multiplying a $d \times d$ matrix by a $d \times 1$ vector, which has a time complexity of $\mathcal{O}(d^2)$. For `MonteCLoRA`, this is $\mathcal{O}(r^2)$.

Thus, sampling one random variable from this multivariate normal distribution has a time complexity of $\mathcal{O}(r^2)$. Since we need to sample n_{in} random variables for a weight matrix, the total time complexity for sampling is $\mathcal{O}(n_{\text{in}}r^2)$.

A.4.4 TOTAL SAMPLING COMPLEXITY FOR THE ENTIRE MODEL

Combining the time complexities for the three sampling steps mentioned above, the time complexity for sampling in one layer is,

$$\mathcal{O}(r^3 + n_{\text{in}}r^2 + N + n_{\text{in}}r^2),$$

which simplifies to

$$\mathcal{O}(n_{\text{in}}r^2 + N),$$

assuming that $r \ll \max(n_{\text{in}}, n_{\text{out}})$. Let M_{in} be the largest input dimension for any layer in the model, and let the number of `MonteCLoRA`-enhanced layers be L_{mc} . The total time complexity for sampling across all layers is,

$$\mathcal{O}(L_{\text{mc}}(n_{\text{in}}r^2 + N)).$$

Since n_{in} is typically constant for most models, the total time complexity is primarily governed by the number of `MonteCLoRA` layers, L_{mc} , and the LoRA rank, r .